

Smooth Flow Matching

Jianbin Tan

Department of Biostatistics & Bioinformatics,
Duke University, Durham, NC, USA

and

Anru R. Zhang*

Department of Biostatistics & Bioinformatics
and Department of Computer Science,
Duke University, Durham, NC, USA

Abstract

Functional data, i.e., smooth random functions observed over a continuous domain, are increasingly available in areas such as biomedical research, health informatics, and epidemiology. However, effective statistical analysis for functional data is often hindered by challenges such as privacy constraints, sparse and irregular sampling, infinite dimensionality, and non-Gaussian structures. To address these challenges, we introduce a novel framework named Smooth Flow Matching (SFM), tailored for generative modeling of functional data to enable statistical analysis without exposing sensitive real data. Built upon flow-matching ideas, SFM constructs a semiparametric copula flow to generate infinite-dimensional functional data, free from Gaussianity or low-rank assumptions. It is computationally efficient, handles irregular observations, and guarantees the smoothness of the generated functions, offering a practical and flexible solution in scenarios where existing deep generative methods are not applicable. Through extensive simulation studies, we demonstrate the advantages of SFM in terms of both synthetic data quality and computational efficiency. We then apply SFM to generate clinical trajectory data from the MIMIC-IV patient electronic health records (EHR) longitudinal database. Our analysis showcases the ability of SFM to produce high-quality surrogate data for downstream statistical tasks, highlighting its potential to boost the utility of EHR data for clinical applications.

Keywords: Copula process, continuous normalizing flow, functional data, generative model, synthetic data analysis

*Email of correspondence: anru.zhang@duke.edu

1 Introduction

Functional data, comprising sequential observations over a continuous domain, have become increasingly prevalent in scientific domains such as biomedical research (Shi et al., 2024; Happ and Greven, 2018), health informatics (Ohalete et al., 2024; Tan et al., 2024b), epidemiology (Carroll et al., 2020; Luo et al., 2025), and spatio-temporal analysis (Tan et al., 2024a). Many of these fields, particularly those involving individual-, institutional-, or regional-level data, often deal with sparse and irregular observations and require secure data sharing. These constraints limit data quality and availability, posing significant challenges for effective analysis of functional data. To address these challenges, generative models offer a principled approach to learning the underlying mechanisms of data, enabling the synthesis of realistic surrogate observations and boosting data utility for statistical analysis (Yoon et al., 2023; Gonzales et al., 2023; Shen et al., 2023; Tian et al., 2024; Golda et al., 2024; Wu et al., 2025). These models facilitate key tasks such as uncertainty quantification and statistical modeling under privacy constraints, demonstrating strong potential for advancing generative modeling in the context of functional data.

Generative modeling for functional data is a more challenging topic than for traditional multivariate tabular data, as the observations are often smooth random curves residing in infinite-dimensional spaces (Ramsay and Silvermann, 2005; Hsing and Eubank, 2015). To account for these characteristics, a widely adopted framework is the Karhunen–Loève (KL) expansion, which models a random function by decomposing it into the sum of a smooth mean function, orthonormal eigenfunctions, and uncorrelated random scores (Ramsay and Silvermann, 2005; Hsing and Eubank, 2015). However, the KL expansion often struggles when functions are sparsely and irregularly observed, which leads to inaccuracy in score estimations arising from the limited and unaligned observations (Yao et al., 2005). To

address this, it is common to assume that functional data possess a low-rank structure and are realizations of Gaussian processes (James et al., 2000; Yao et al., 2005; Yao, 2007). This assumption enables accurate estimation under sparse and irregular designs, providing a potential solution for the generative modeling of functional data.

Despite the success of Gaussian-based methods, their crucial limitation is the reliance on the Gaussian assumption, which captures only the mean and covariance signals of the data and may not hold in practice—particularly for functional data exhibiting heavy-tailed distributions. In addition, the low-rank assumption may impose unnecessary restrictions on the underlying structure, conflicting with the infinite-dimensional nature of functional data and limiting the expressiveness of generative approaches. A relaxation of these assumptions is offered by the copula process framework (Wilson and Ghahramani, 2010), which models the joint distribution of random functions by decomposing it into two components: the marginal distributions and a copula that captures functional dependencies. However, existing copula-based methods typically rely on parametric forms for the marginals or assume dense and regular sampling of functional data (Staicu et al., 2012; Zhang et al., 2022), limiting their applicability in sparse and irregular settings as well as for data with general marginals.

Recently, another line of research has focused on deep generative models for functional data, offering flexible nonparametric approaches for synthesizing new data samples from infinite-dimensional spaces. One framework for generative models is based on score-based techniques (Lim et al., 2023; Kerrigan et al., 2023; Franzese et al., 2023), which generalize score functions for random vectors (Vincent, 2011; Song and Ermon, 2019) to the setting of random functions. Using scores estimated by deep learning (LeCun et al., 2015), these methods generate new functional data by starting with random noise and guiding it through

a probabilistic flow induced by the score. Another framework, instead, builds on more general flow-based techniques using vector fields (Lipman et al., 2023; Liu et al., 2022; Tong et al., 2024). A representative example of flow-based methods is functional flow matching (Kerrigan et al., 2024), which extends the concepts of flows and vector fields to accommodate infinite-dimensional functions. This method employs deep learning to estimate the vector fields from observed data, under which random noise is transformed into new samples via a continuous flow directed by the vector field (Chen et al., 2018).

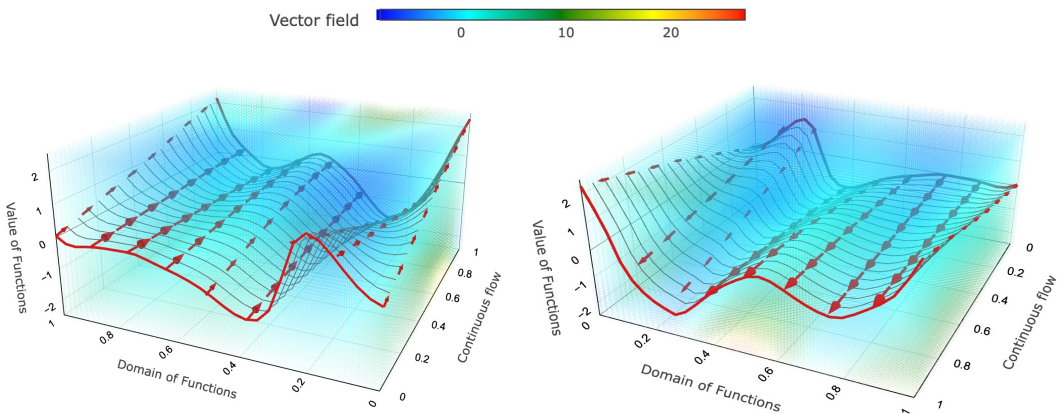


Figure 1: A pictorial illustration of functional data generation via three-dimensional flow. The left panel shows the base function input into the flow, while the right panel displays the output functions generated by applying the base functions through the flow transformation.

While the above methods offer flexibility, they generally require the functional data to be fully (or at least densely) observed over the entire domain. This requirement is often impractical in real-world scenarios, where observation times are typically irregular across subjects and often sparse (Yao et al., 2005; Wang et al., 2016; Nie et al., 2022; Tan et al., 2024b). Moreover, the score and vector field concepts in these frameworks are typically formulated as operators between function spaces (Lim et al., 2023; Kerrigan et al., 2024), which are complex objects that require substantial data and incur high estimation costs.

These operator are mostly modeled using deep neural networks, , which further reduces interpretability in the data-generation process. Finally, existing deep generative models for functional data provide no guarantee of smoothness in the generated functions. This deficiency may result in a loss of statistical efficiency and lead to unreasonable non-smooth generations.

To address the above issues, we propose a novel generative method, **Smooth Flow Matching** (SFM), tailored for generating new functional samples from irregularly or sparsely observed functional data. Our method adopts a copula-based generation framework using flow-based techniques, capable of producing non-Gaussian and heavy-tailed functional data without relying on the low-rank assumption. The SFM framework is built on a novel functional-form flow, enabling data generation through a smooth three-dimensional vector field rather than high-dimensional operator-based generators as in [Lim et al. \(2023\)](#); [Kerrigan et al. \(2024\)](#). This construction is significantly simpler without the use of deep neural networks and more interpretable than existing flow-based and score-based methods, allowing for computationally efficient generation of functional data while ensuring the smoothness of synthetic samples. A flowchart illustrating the three-dimensional vector fields is provided in Figure 1.

Overall, SFM provides several advantages over existing deep generative models as well as Gaussian-based methods. First, SFM utilizes flow-based techniques to estimate marginal distributions of random functions rather than their full joint distribution, enabling direct flow estimation from irregular and sparse functional data. This procedure retains the nonparametric flexibility of the marginals to capture distributional features beyond the mean and covariance, while avoiding the high computational cost and dense observation requirements of full joint modeling in deep generative methods. Second, SFM naturally

incorporates smoothness into the flow estimation, allowing it to borrow strength across curves and produce smooth functional data from sparse or irregular samples—analogous to the mean and covariance estimation in Gaussian-based approaches (Yao et al., 2005; Yao, 2007). With the estimated smooth flow, we can directly construct its inverse flow to transport the data to latent copula observations. This method provides a flexible and interpretable semiparametric framework for functional data generation. We summarize the comparisons of our method to others in Table 1.

Table 1: Comparison of SFM with other methods for functional data

Name	Deep Models (Lim et al., 2023; Kerrigan et al., 2024)	Generative Gaussian-based Methods (Yao et al., 2005; Yao, 2007)	Smooth Matching (this work)	Flow
Data Resolution	Dense	Dense or sparse	Dense or sparse	
Computational Cost	High	Relatively low	Relatively low	
Interpretability	May be relatively low	High	High	
Guaranteed Smoothness	No	Yes	Yes	
Joint Distribution	Nonparametric	Parametric	Semiparametric	

To demonstrate the utility of SFM, we provide statistical consistency of the proposed methods under a practical sparse and irregular design of functional data. Furthermore, we compare SFM with existing deep generative methods and Gaussian-based methods through extensive simulation studies, examining both Gaussian process and heavy-tailed process scenarios. Our results show that SFM performs better than existing methods in both cases while significantly reducing computational cost compared to deep generative methods.

Finally, we apply SFM to synthetic clinical trajectory data from the MIMIC-IV pa-

tient electronic health records (EHR) longitudinal database (Johnson et al., 2024), where observation times across patients are typically irregular and often sparse. Our analysis shows that SFM effectively recovers the dominant longitudinal patterns and key distributional features of the original EHR data. We further evaluate the synthetic performance of SFM through a data prediction task, where SFM-generated data exhibit superior predictive power compared to data generated by other methods. These results demonstrate the advantage of SFM in producing high-quality surrogate EHR data for downstream statistical tasks.

The rest of this paper is organized as follows. In Section 2, we introduce the copula flow framework for functional data. After a brief discussion of the notation, we introduce copula functional data in Section 2.1, discuss the continuous normalizing flow for functional data in Section 2.2, and examine the smoothness properties of continuous normalizing flow in Section 2.3. We then propose the estimation of flows and data generation using SFM in Sections 3 and 4, respectively focusing on fully observed and on sparse, irregularly observed functional data, with a demonstration of statistical consistency in Section 4.3. In Section 5, we perform an extensive simulation study comparing SFM with existing generative methods. Section 6 applies SFM to synthetic trajectory data from electronic health record longitudinal data. We conclude with a discussion in Section 7.

2 Copula Flow for Functional Data

Denote $L^2(\mathcal{T})$ as the space of square-integrable functions from \mathcal{T} to \mathbb{R} , equipped with the L^2 norm $\|\cdot\|$ and the inner product $\langle \cdot, \cdot \rangle$, where $\mathcal{T} \subset \mathbb{R}$ is compact. For any vector $\mathbf{a} = (a_1, \dots, a_n)^\top$, we also denote its L^2 norm by $\|\mathbf{a}\| := \sqrt{\sum_{i=1}^n a_i^2}$. For a right-continuous increasing function F , define its generalized inverse by $F^{-1}(y) = \inf\{u : F(u) \geq y\}$. Let

$\mathbb{I}(\cdot)$ denote the indicator function. We use “ $\stackrel{d}{=}$ ” to denote equality in distribution, and Φ denotes the cumulative distribution function (CDF) for the standard normal distribution. Let $\mathcal{N}(a, b)$ denote the normal distribution with mean a and variance b . The support of a continuous random variable X is denoted by $\text{supp}(X)$. In what follows, we may abbreviate a functional object or stochastic process $f(\cdot)$ simply as f .

In this section, we develop a copula-based normalizing flow framework for modeling a random function X , with the goal of generating new functional samples that have the same distribution as X . In short, we construct a continuous family of maps $\{\phi_{u,t}(\cdot) : u \in [0, 1]\}$ that connects the functional data X to a base stochastic process Z with a simple distribution (mostly Gaussian process in practice). That is $\phi_{0,t}(Z(t)) \stackrel{d}{=} Z(t)$ and $\phi_{1,t}(Z(t)) \stackrel{d}{=} X(t)$, $t \in \mathcal{T}$. To this end, we establish a vector field $V_{u,t}$ to generate the map $\phi_{u,t}(\cdot)$ sequentially, which approximately achieves

$$\phi_{u+\Delta u,t}(x) \approx \phi_{u,t}(x) + V_{u,t}(\phi_{u,t}(x)) \cdot \Delta u,$$

where Δu represents a small increment. This sequential formulation enables the construction of expressive maps $\phi_{u,t}(\cdot)$ that can capture complex data distributions while ensuring the generation of smooth functional data. Next, we outline general principles of copula-based functional data in Section 2.1, and then introduce a continuous normalizing flow framework for modeling and data generation in Sections 2.2 – 2.3.

2.1 Copula Functional Data

Denote the marginal distribution of $X(t)$ as $F_t(x)$, $t \in \mathcal{T}$ and $x \in \mathbb{R}$. The copula of $X(\cdot)$ is essentially a joint cumulative distribution function c , in the sense that for any $t_1, \dots, t_m \in \mathcal{T}$ and $u_1, \dots, u_m \in [0, 1]$,

$$c_{t_1, \dots, t_m}(u_1, \dots, u_m) := \mathbb{P}(F_{t_1}(X(t_1)) \leq u_1, \dots, F_{t_m}(X(t_m)) \leq u_m). \quad (1)$$

Note that $F_{t_1}(X(t_1)), \dots, F_{t_m}(X(t_m))$ are uniformly distributed random variables, whose joint distribution, the copula, determines the dependence structure among the random variables $X(t_1), \dots, X(t_m)$. The copula framework provides a flexible approach for separately modeling the marginal distributions of $X(t_1), \dots, X(t_m)$ and their dependence structure. This separation is particularly useful when direct modeling of the joint distribution of X is difficult.

A common approach to modeling the copula is through a latent variable representation called copula process ([Wilson and Ghahramani, 2010](#)). See the following definition.

Definition 1 (Copula Process). X is a copula process with a base process Z if for any $t_1, \dots, t_m \in \mathcal{T}$ and $u_1, \dots, u_m \in [0, 1]$,

$$c_{t_1, \dots, t_m}(u_1, \dots, u_m) = H_{\text{base}}(F_{t_1, \text{base}}^{-1}(u_1), \dots, F_{t_m, \text{base}}^{-1}(u_m); t_1, \dots, t_m),$$

where $F_{t, \text{base}}$, $t \in \mathcal{T}$, are the marginal distributions of Z , and $H_{\text{base}}(\cdot; t_1, \dots, t_m)$ is the joint distribution of $Z(t_1), \dots, Z(t_m)$.

The definition indicates that the copula of X is determined by a latent base process Z . If $X(t)$ is a continuous random variable, $t \in \mathcal{T}$, we have

$$\begin{aligned} & H_{\text{base}}(h_1, \dots, h_m; t_1, \dots, t_m) \\ &= \mathbb{P}(F_{t_1, \text{base}}^{-1} \circ F_{t_1}(X(t_1)) \leq h_1, \dots, F_{t_m, \text{base}}^{-1} \circ F_{t_m}(X(t_m)) \leq h_m), \end{aligned} \quad (2)$$

for $h_1 \in \text{supp}(Z(t_1)), \dots, h_m \in \text{supp}(Z(t_m))$, which implies that the distribution of Z can be extracted by X through the transformations $F_{t, \text{base}}^{-1} \circ F_t$, $t \in \mathcal{T}$.

The concept of copula processes has been employed in the modeling of functional data in literature ([Staicu et al., 2012](#); [Zhang et al., 2022](#)). A commonly used base for copula processes is the Gaussian distribution (see the example below). More general bases, such

as the Student- t distribution, can also been adopted for copula processes; see Part B.2 of the Supplementary Materials for more details.

Example 1 (Gaussian Copula Process). *Let $\Phi_\rho(\cdot; t_1, \dots, t_m)$ denote the joint distribution function of a mean-zero Gaussian process evaluated at t_1, \dots, t_m , with a covariance function ρ . When $F_{t, \text{base}}$ is taken as Φ , $t \in \mathcal{T}$ and $H_{\text{base}}(\cdot; t_1, \dots, t_m) = \Phi_\rho(\cdot; t_1, \dots, t_m)$, $t_1, \dots, t_m \in \mathcal{T}$, we refer to $X(\cdot)$ as a Gaussian copula process with latent correlation function ρ . It is worth noting that a Gaussian copula process X satisfies that $\Phi^{-1} \circ F_t(X(t))$, for $t \in \mathcal{T}$, is a Gaussian process with covariance function ρ . This means*

$$\rho(t, s) = \mathbb{E}\{\Phi^{-1} \circ F_t(X(t))\} \cdot \{\Phi^{-1} \circ F_s(X(s))\}, \quad t, s \in \mathcal{T}. \quad (3)$$

A copula process can be generated via the transportation of a latent process, as stated below.

Proposition 1 (An Equivalent Condition for Copula Processes). *Assume $X(t)$ and $Z(t)$ are continuous random variables, $t \in \mathcal{T}$. $X(\cdot)$ is a copula process with a base $Z(\cdot)$ if and only if there exists a family of continuous and strictly increasing functions $\{g_t: \text{supp}(Z(t)) \rightarrow \text{supp}(X(t))\}_{t \in \mathcal{T}}$ such that the two stochastic processes $\{X(t)\}_{t \in \mathcal{T}}$ and $\{g_t(Z(t))\}_{t \in \mathcal{T}}$ are equal in distribution.*

Proposition 1 shows that the Gaussian process $X(t) = \mu(t) + \sigma(t)Z(t)$, the log-Gaussian process $X(t) = \exp\{\mu(t) + \sigma(t)Z(t)\}$, and skewed processes of the form $X(t) = \mu(t) + \sigma(t)G^{-1}(\Phi(Z(t)))$ are all special cases of Gaussian copula processes. Here, $Z(\cdot)$ is any Gaussian process such that $Z(t) \sim \Phi$, $t \in \mathcal{T}$, $\mu(t)$ and $\sigma(t)$ are fixed functions with $\sigma(t) > 0$, $\forall t \in \mathcal{T}$, and G is a cumulative distribution function from a parametric family with zero mean, unit variance, and a shape parameter. These processes have been proposed for modeling functional data in the literature (Yao et al., 2005; Staicu et al., 2012), typically focusing on capturing low-order moments such as the mean, covariance, and skewness.

More generally, processes of the form

$$X(t) := F_t^{-1} \circ F_{t,\text{base}}(Z(t)), \quad t \in \mathcal{T} \quad (4)$$

are also copula processes with a base Z , where F_t can be any continuous and strictly increasing distribution functions on $\text{supp}(X(t))$, $t \in \mathcal{T}$. This indicates that the copula process can capture rich marginal distributional characteristics beyond low-order moments.

2.2 Continuous Normalizing Flow for Functional Data

In this subsection, we introduce the basic framework for generating copula-based functional data. Following (4), new functional data can be generated in two steps: first, sample a base function Z from the joint distribution $H_{\text{base}}(\cdot)$; then, generate a new functional sample by applying the transformation $F_t^{-1} \circ F_{t,\text{base}}(Z(t))$ for each $t \in \mathcal{T}$. This approach relies on two key components: the joint distribution $H_{\text{base}}(\cdot)$ and the transformation $F_t^{-1} \circ F_{t,\text{base}}$. Due to (2), $H_{\text{base}}(\cdot)$ is further determined by the observed process X after transformation via $F_{t,\text{base}}^{-1} \circ F_t$. Therefore, both maps

$$F_{t,\text{base}}^{-1} \circ F_t \quad \text{and} \quad F_t^{-1} \circ F_{t,\text{base}}$$

play essential roles in generating copula-based functional data.

We propose to characterize both $F_t^{-1} \circ F_{t,\text{base}}$ and $F_{t,\text{base}}^{-1} \circ F_t$, as well as the generation of copula functional data, within the framework of continuous normalizing flows (Chen et al., 2018). Specifically, we construct a flow map $\phi_{u,t}$ such that

$$\phi_{u,t}(Z_0(t)) = Z_u(t), \quad t \in \mathcal{T}, \quad u \in [0, 1], \quad (5)$$

where Z_u , $u \in [0, 1]$, is a sequence of random functions on \mathcal{T} that satisfies: Z_0 is a base process with the joint distribution $H_{\text{base}}(\cdot)$, and Z_1 is the target function such that $Z_1(t) \stackrel{d}{=}$

$X(t)$, $t \in \mathcal{T}$. We want the flow map $\phi_{u,t}$ satisfying

$$\phi_{0,t}(\cdot) = \text{id}(\cdot), \quad \phi_{1,t}(\cdot) = F_t^{-1} \circ F_{t,\text{base}}(\cdot), \quad t \in \mathcal{T}, \quad (6)$$

which facilitates the extraction of $F_t^{-1} \circ F_{t,\text{base}}$ and $F_{t,\text{base}}^{-1} \circ F_t$ by the flow, and ensures that the stochastic processes Z_1 and X are equal in distribution (see the demonstration below).

In the following, we construct $\{\phi_{u,t}; u \in [0, 1]\}$ to accomplish (6) using continuous normalizing flows and vector fields.

Definition 2 (Vector Field for Continuous Normalizing Flow). Consider a u, t -dependent vector field $V_{u,t}(\cdot)$ from \mathbb{R} to \mathbb{R} and a diffeomorphic map $\phi : [0, 1] \times \mathcal{T} \times \mathbb{R} \rightarrow \mathbb{R}$ induced by $V_{u,t}$:

$$\frac{\partial \phi_{u,t}(x)}{\partial u} = V_{u,t}(\phi_{u,t}(x)) \quad \text{subject to} \quad \phi_{0,t}(x) = x. \quad (7)$$

For a functional sequence $\{Z_u; u \in [0, 1]\}$, denote $p_{u,t}(\cdot)$ as the probability density function of $Z_u(t)$. We say the vector field $V_{u,t}$ generates $\{Z_u; u \in [0, 1]\}$ or the probability path $\{p_{u,t}; u \in [0, 1], t \in \mathcal{T}\}$ if the map $\phi_{u,t}$ satisfies

$$\phi_{u,t}(Z_0(t)) = Z_u(t) \quad \text{or equivalently} \quad p_{u,t}(x) = p_{0,t}(\phi_{u,t}^{-1}(x)) \cdot \left| \frac{\partial \phi_{u,t}^{-1}(x)}{\partial x} \right|$$

for $u \in [0, 1]$ and $t \in \mathcal{T}$.

In Definition 2, the vector field $V_{u,t}$ establishes a flow map $\phi_{u,t}(\cdot)$ for each t , transporting $Z_0(t)$ to $Z_u(t)$ via the differential equation (7). This definition guarantees that $\phi_{0,t}(\cdot) = \text{id}(\cdot)$ and $\phi_{1,t}(Z_0(t)) \stackrel{d}{=} F_t^{-1} \circ F_{t,\text{base}}(Z_0(t))$, $t \in \mathcal{T}$, when Z_0 and Z_1 have marginal distributions $F_{t,\text{base}}$ and F_t , respectively. The following theorem establishes the existence and uniqueness of the solution to (7), which ensures that (6) holds.

Theorem 1 (Existence and Uniqueness of Solution to (7)). Assume that the vector field $V_{u,t}(x)$ is uniformly bounded for $u \in [0, 1]$, $t \in \mathcal{T}$, and $x \in \mathbb{R}$, and is continuous in $u \in D$.

Moreover, suppose for any $x, y \in \mathbb{R}$ and $t \in \mathcal{T}$,

$$|V_{u,t}(x) - V_{u,t}(y)| \leq L \cdot |x - y|$$

for some Lipschitz constant L independent of u , x , y , and t . Then:

- (a) There exists a unique functional sequence $\{Z_u; u \in (0, 1]\}$ generated by Z_0 and $V_{u,t}$.
- (b) The flow map $\phi_{1,t}$ is invertible for any $t \in \mathcal{T}$, and its inverse $\phi_{1,t}^{-1}$ satisfies $\phi_{1,t}^{-1} = \psi_{1,t}$,
 $t \in \mathcal{T}$, where $\{\psi_{u,t}; u \in [0, 1]\}$ is the solution of

$$\frac{\partial \psi_{u,t}(z)}{\partial u} = -V_{1-u,t}(\psi_{u,t}(z)) \quad \text{with} \quad \psi_{0,t}(z) = z, \quad (8)$$

for each t and $z \in \{\phi_{1,t}(x); x \in \mathbb{R}\}$.

- (c) Suppose $Z_0(t)$ and $Z_1(t)$ are continuous random variables, $t \in \mathcal{T}$. Let the marginal distributions of $Z_0(t)$ and $Z_1(t)$ be $F_{t,\text{base}}$ and F_t , respectively. Then, for each $t \in \mathcal{T}$, $\phi_{1,t}(\cdot)$ and $\psi_{1,t}(\cdot)$ satisfy

$$\phi_{1,t}(z) = F_t^{-1} \circ F_{t,\text{base}}(z) \quad \text{and} \quad \psi_{1,t}(x) = F_{t,\text{base}}^{-1} \circ F_t(x),$$

for Lebesgue-almost every $z \in \text{supp}(Z_0(t))$ and $x \in \text{supp}(Z_1(t))$.

- (d) Under the conditions in (c), suppose that X is a copula process with marginals F'_t , $t \in \mathcal{T}$, and Z_0 is the base of X . If $F'_t = F_t$ for all $t \in \mathcal{T}$, then X and Z_1 are equal in distribution.

Theorem 1 indicates that, under mild conditions, $\phi_{1,t}$ is the unique solution to (7) for all $t \in \mathcal{T}$. This guarantees that $\phi_{1,t}^{-1} = \psi_{1,t}$ exists and can be constructed via (8) using the vector field $V_{u,t}$. As a result, (6) holds, and both maps $F_t^{-1} \circ F_{t,\text{base}}$ and $F_{t,\text{base}}^{-1} \circ F_t$ can be generated by V under the continuous normalizing flow framework (Theorem 1(c)). The property leads to valid generation of Z_1 with the same distribution as X , as ensured by Theorem 1(d).

Remark 1 (Flow Models via Continuous Normalizing Flows). *Continuous normalizing flows are a flexible subclass of normalizing flow models capable of representing highly complex data distributions (Papamakarios et al., 2021). They offer several key advantages for flow modeling. First, the map $\phi_{u,t}(\cdot)$ induced by differential equations is always a diffeomorphism, thereby ensuring invertibility throughout the transformation to obtain desirable properties. Second, the use of infinitesimal vector fields in (7) allows for an infinite sequence of nonlinear transformations, which provides high expressive power to approximate a broad class of target distributions. Finally, estimating continuous flows is straightforward and computationally efficient: it can be solved by a simple least-squares via flow-matching procedures described in Section 3.*

Remark 2 (Continuous Normalizing Flows for Functional Data Generation). *Unlike existing normalizing flows which require estimating only the forward map from a base to a target, we require estimating both the forward map $F_t^{-1} \circ F_{t,base}$ and the backward map $F_{t,base}^{-1} \circ F_t$ for copula functional data generation. This makes continuous normalizing flows particularly well-suited for this task, as both maps can be obtained from (7) or (8) via the same vector field $V_{u,t}$. Moreover, the continuous normalizing flow framework is especially useful in settings where functional observations are irregular and sparse, as discussed in Section 4. In such cases, it is challenging to construct reliable estimators for both $F_t^{-1} \circ F_{t,base}$ and $F_{t,base}^{-1} \circ F_t$, while also ensuring that the generated data exhibit realistic features such as smooth trajectories. We will show that continuous normalizing flows provide an effective solution to these challenges.*

2.3 Smooth Flow

In this subsection, we specifically focus on generating smooth functions using continuous normalizing flows. To characterize the smoothness of such functions, we consider the Sobolev space $W_q^2(\mathcal{T}) := \{f : \mathcal{T} \rightarrow \mathbb{R} \mid f^{(j)} \in L^2(\mathcal{T}) \text{ for all } 0 \leq j \leq q\}$, which consists of functions whose derivatives up to order q exist and are square-integrable over \mathcal{T} . Sobolev spaces are a widely adopted framework for modeling smooth random functions (Yuan and Cai, 2010; Hsing and Eubank, 2015).

Recall the continuous normalizing flow model (Definition 2) solves the differential equation to generate new functional samples:

$$\frac{\partial Z_u(t)}{\partial u} = V_{u,t}(Z_u(t)), \quad t \in \mathcal{T}, \quad (9)$$

given the initial condition $Z_0(t)$. We propose the following theorem to ensure that the solution to (9) lies in the Sobolev space $W_q^2(\mathcal{T})$.

Theorem 2 (Smooth Function Generation via Smooth Flow). Suppose the conditions in Theorem 1. For $u \in [0, 1]$, the order- q partial derivatives of $V_{u,t}(x)$ with respect to t and x exist, and

$$\frac{\partial^{l+m} V_{u,t}(x)}{\partial t^m \partial x^l} \in L^2(\mathcal{T}), \quad (10)$$

for all $l + m = q$. Then, for any $h(\cdot) \in W_q^2(\mathcal{T})$, we have $V_{u,\cdot}(h(\cdot)) \in W_q^2(\mathcal{T})$.

Furthermore, if $\|V_{u,\cdot}(h(\cdot))\|_{W_q^2(\mathcal{T})}$ is uniformly bounded for all $u \in [0, 1]$ and $h \in W_q^2(\mathcal{T})$; for any $h_1, h_2 \in W_q^2(\mathcal{T})$,

$$\|V_{u,\cdot}(h_1(\cdot)) - V_{u,\cdot}(h_2(\cdot))\|_{W_q^2(\mathcal{T})} \leq L_{W_q^2(\mathcal{T})} \cdot \|h_1 - h_2\|_{W_q^2(\mathcal{T})}, \quad (11)$$

where $\|\cdot\|_{W_q^2(\mathcal{T})}$ denotes any valid norm on the Sobolev space and $L_{W_q^2(\mathcal{T})}$ is a constant independent of u , h_1 , and h_2 . Then the theoretical solution Z_u to (9) lies in $W_q^2(\mathcal{T})$, provided that $Z_0 \in W_q^2(\mathcal{T})$.

In Theorem 2, (10) ensures that $\frac{\partial Z_u}{\partial u} \in W_q^2(\mathcal{T})$ whenever $Z_u \in W_q^2(\mathcal{T})$, which implies that $Z_u + \Delta u \cdot \frac{\partial Z_u}{\partial u} \in W_q^2(\mathcal{T})$ for any sufficiently small increment Δu . Given this, the functional Lipschitz condition (11) guarantees that $\lim_{\Delta u \rightarrow 0} (Z_u + \Delta u \cdot \frac{\partial Z_u}{\partial u})$ exists and lies in $W_q^2(\mathcal{T})$, ensuring that the solution to (9) remains in $W_q^2(\mathcal{T})$.

In practice, we need to approximate the solution of (9) using numerical methods. Proposition S1 of the Supplementary Materials shows that condition (10) is sufficient to guarantee that the numerical solution to (9), in particular the Runge–Kutta method (a widely used numerical technique in ordinary differential equation literature ([Butcher, 1996](#))), lies in $W_q^2(\mathcal{T})$.

Example 2 (Gaussian Bases with Smooth Covariance Functions). *If $Z_0(\cdot)$ is a mean-zero Gaussian process with covariance function K , with K being a positive-definite kernel such that $\frac{\partial^{2q} K(t,s)}{\partial t^q \partial s^q}$ exists and is continuous on $\mathcal{T} \times \mathcal{T}$. Then the realizations of $Z_0(\cdot)$ belong to the Sobolev space $W_2^q(\mathcal{T})$ almost surely ([Henderson, 2024](#)), which satisfies the requirement in Theorem 2.*

3 Flow Matching for Copula Functional Data

Suppose $X(t)$ and $Z_u(t)$, with $u \in [0, 1]$ and $t \in \mathcal{T}$, are continuous random variables. Here, X represent a random function and $\{Z_u; u \in [0, 1]\}$ is any random functional sequence with the probability path $\{p_{u,t}; u \in [0, 1], t \in \mathcal{T}\}$. Denote the probability density function of $X(t)$ as $f_X(\cdot; t)$.

In this section, we consider $X(\cdot)$ to be a copula process on \mathcal{T} with some base process Z_0 , and aim to extract vector fields based on the random function X such that $Z_1(t) \stackrel{d}{=} X(t)$, $t \in \mathcal{T}$. To achieve this goal, we propose to apply flow matching ([Lipman et al., 2023](#)) for functional data. Specifically, given $\{Z_u; u \in [0, 1]\}$ satisfying $Z_1(t) \stackrel{d}{=} X(t)$, $t \in \mathcal{T}$, the

objective of flow matching is to solve

$$\min_U \int_0^1 \mathbb{E} \left\{ \frac{\partial Z_u(T)}{\partial u} - U(u, t, Z_u(T)) \right\}^2 du, \quad (12)$$

where U is a three-dimensional function on $[0, 1] \times \mathcal{T} \times \mathbb{R}$, and T is a random variable independent of Z_u s, which take values in \mathcal{T} with a density that is bounded away from zero. Since $\frac{\partial Z_u(t)}{\partial u} = V_{u,t}(Z_u(t))$ by (7), the minimizer of $U(u, t, x)$ in (12) is the vector field $V_{u,t}(x)$, for $u \in [0, 1]$, $t \in \mathcal{T}$, and $x \in \text{supp}(Z_u(t))$, almost everywhere. In the following, we propose to solve the flow matching problem (12) while bypassing the need to solve differential equations in flow estimation.

3.1 Conditional Flow Matching

The flow matching objective (12) is intractable if the functional sequence $\{Z_u; u \in [0, 1]\}$ is unknown. To address this, we extend the conditional probability path approach (Lipman et al., 2023; Tong et al., 2024) to the functional data setting, relying on the construction of a conditional probability path to induce the sequence $\{Z_u; u \in [0, 1]\}$. Specifically, given $X(t)$, let $p_{u,t}(\cdot | X(t))$ denote a conditional probability density which satisfies

$$p_{0,t}(\cdot | X(t)) = p_{0,t}(\cdot) \quad \text{and} \quad p_{1,t}(\cdot | X(t)) = \delta(\cdot; X(t)), \quad t \in \mathcal{T}. \quad (13)$$

Here, $\delta(\cdot; \cdot)$ is the Dirac measure. Given $p_{u,t}(\cdot | x)$ and $f_X(x; t)$, we define a marginal probability path $p_{u,t}(\cdot)$:

$$p_{u,t}(\cdot) := \int_{\mathbb{R}} p_{u,t}(\cdot | x) \cdot f_X(x; t) dx. \quad (14)$$

Then, $p_{1,t}(\cdot) = f_X(\cdot; t)$ by combining (13) and (14), which means $\{p_{u,t}; u \in [0, 1], t \in \mathcal{T}\}$ pushes the density $p_{0,t}(\cdot)$ toward $f_X(\cdot; t)$ as u varies from 0 to 1. We will specify the construction of $p_{u,t}(\cdot | x)$ that satisfies (13) in the next subsection.

The following lemma shows that the flow matching in (12) is equivalent to the flow matching in (16) with the conditional path.

Theorem 3. Given any random function $X(t)$ with probability density $f_X(x; t)$ and any initial probability density $p_{0,t}(\cdot)$, let $V_{u,t}(\cdot \mid X(t))$ be a vector field to generate the conditional probability path $\{p_{u,t}(\cdot \mid X(t)); u \in [0, 1]\}$, $t \in \mathcal{T}$. Denote the support of $p_{u,t}$ in (14) as $\text{supp}(p_{u,t})$ and define

$$V_{u,t}(\cdot) = \int_{\text{supp}(p_{u,t})} V_{u,t}(\cdot \mid x) \cdot \frac{p_{u,t}(\cdot \mid x) \cdot f_X(x; t)}{p_{u,t}(\cdot)} dx. \quad (15)$$

Suppose that $V_{u,t}$ satisfies the conditions in Theorem 1.

If $\{Z_u(t); u \in [0, 1]\}$ is generated by $V_{u,t}$ in (15) with $Z_0(t) \sim p_{0,t}$, then $Z_u(t) \sim p_{u,t}$, $u \in [0, 1]$ and $t \in \mathcal{T}$. As a result, the minimizers U obtained from (12) based on the functional sequence $\{Z_u(t) : u \in [0, 1]\}$, and from

$$\min_U \int_0^1 \mathbb{E} \left\{ \mathbb{E} \left(\frac{\partial Z_u(T)}{\partial u} - U(u, t, Z_u(T)) \right)^2 \mid X, T \right\} du. \quad (16)$$

with $Z_u(t) \mid X(t) \sim p_{u,t}(\cdot \mid X(t))$, are the same.

Two important points are worth noting regarding the optimization (16). First, we only require the marginal density $p_{0,t}$, $t \in \mathcal{T}$, to construct the conditional path $p_{u,t}(\cdot \mid X(t))$, so full knowledge of the joint distribution of Z_0 is not necessary for vector field estimation. Second, the construction of Z_u , $u \in [0, 1]$, in (16) depends only on X and $p_{0,t}$, and is independent of the vector field $V_{u,t}$. This independence makes Z_u free from $V_{u,t}$. Therefore, we do not need to solve the differential equation (7) to obtain Z_u given $V_{u,t}$. This procedure bypasses the computationally intensive task of solving differential equations, allowing us to directly match the differential equation (7) for estimating $V_{u,t}$. Such equation-matching strategy can also be found in the literature for ordinary differential equation estimation (Ramsay and Hooker, 2017; Tan et al., 2024c).

3.2 Constructing a Conditional Path

To implement conditional flow matching, we need to specify the path $\{p_{u,t}(\cdot \mid X(t)) : u \in [0, 1], t \in \mathcal{T}\}$. Notably, there are infinitely many choices of such conditional paths that satisfy the conditions in (13). This flexibility enables the flow matching framework to encompass a variety of generative models, such as diffusion models (Lipman et al., 2023), as special cases.

In this article, we adopt the rectified flow (Liu et al., 2022) to construct the conditional probability path as a straight-line path connecting $Z_0(t)$ and $X(t)$:

$$p_{u,t}(\cdot \mid X(t)) = \delta(\cdot \mid (1-u)Z_0(t) + uX(t)), \quad Z_0(t) \sim p_{0,t}, \quad t \in \mathcal{T}. \quad (17)$$

The flows induced by (17) allow the base density $p_{0,t}$ to be any general distribution, while retaining desirable transport properties for mapping $p_{0,t}$ to the target density $f_X(\cdot; t)$ (Liu et al., 2022).

Using the rectified flow (17), the conditional flow matching problem (16) becomes

$$\begin{aligned} V : &= \min_U \int_0^1 \mathbb{E} \left[\mathbb{E} \left\{ X(T) - Z_0(T) - U(u, t, Z_u(T)) \right\}^2 \mid X, T \right] du \\ &= \min_U \int_0^1 \mathbb{E} \left\{ X(T) - Z_0(T) - U(u, T, Z_u(T)) \right\}^2 du, \end{aligned} \quad (18)$$

where $Z_0(t) \sim p_{0,t}$, $X(t) \sim f_X(\cdot; t)$, $t \in \mathcal{T}$, and $Z_u(t) = (1-u)Z_0(t) + uX(t)$, $u \in [0, 1]$; Z_0 , X , and T are independent. The flow induced by V yields a valid transport from the distribution of $Z_0(t)$ to that of $X(t)$ (equivalently $Z_1(t)$), for $t \in \mathcal{T}$.

By Theorem 1 (c), the vector field V extracted from (18) can induce the transformations $F_t^{-1} \circ F_{t,\text{base}}$ using continuous normalizing flows, provided that the marginal distributions of Z_0 and Z_1 are taken as $F_{t,\text{base}}$ and F_t , respectively. As a result, we can generate new functional data by solving (9), with $V_{u,t}(x)$ obtain from (18) and the initial conditions

sampled from the base of the copula process X . The generated functions are then identically distributed to X , as ensured by Theorem 1(d).

We can also obtain the inverse map $F_{t,\text{base}}^{-1} \circ F_t$ from the extracted vector field V by solving (8), as guaranteed by Theorem 1(b)–(c). This step is crucial for determining the distribution of the base in data generation. Alternatively, one might estimate the map $F_{t,\text{base}}^{-1} \circ F_t$ directly via flow matching, by setting the base distribution to F_t and the target distribution to $F_{t,\text{base}}$. Theorem S1 in the Supplemental Material shows that these two approaches are equivalent under the rectified flow. Therefore, it suffices to solve (18) to obtain the flow-matching estimates for $F_t^{-1} \circ F_{t,\text{base}}$, $t \in \mathcal{T}$.

4 Smooth Flow Matching

In real-world applications, random functions are only observed at discrete time points rather than being directly measured across the entire continuum (Yao et al., 2005; Chiou and Li, 2007; Wang et al., 2016; Nie et al., 2022; Tan et al., 2024b). This scenario is referred to as the sparsely observed functional data (Yao et al., 2005; Chiou and Li, 2007; Wang et al., 2016; Nie et al., 2022; Tan et al., 2024b). It is conventional to model this type of data as X_i , $i = 1, \dots, n$, which are only observed at times $\{T_{ij} \in \mathcal{T}; j \in [J_i]\}$ for each i . Here, n is the sample size of functional data, J_i s represent the observed number of time points, and $\{T_{ij}; j \in [J_i]\}$ may vary across different subjects i .

Our objective in this section is to establish a flow-matching method for generating new functional samples from irregularly and sparsely observed functional data.

4.1 Flow Matching for Irregular Functional Data

We adopt the flow matching method introduced in Section 3, which pools irregularly observed data across subjects to facilitate the estimation of vector fields. First, we take $Z_0(\cdot)$ as a stochastic process with known marginal distributions $F_{t,\text{base}}$, $t \in \mathcal{T}$, where the copula of $Z_0(\cdot)$ can be arbitrary at this stage. Accordingly, we construct an empirical loss function based on (18) as follows:

$$\mathcal{L}(U) = \frac{1}{n} \sum_{i=1}^n \frac{1}{J_i} \sum_{j=1}^{J_i} \int_0^1 \mathbb{E} \left[\left\{ X_i(T_{ij}) - Z_0(T_{ij}) - U(u, T_{ij}, Z_{u,i}(T_{ij})) \right\}^2 \mid X_i, T_{ij} \right] \mathrm{d}u \quad (19)$$

Here, $U : ([0, 1], \mathcal{T}, \mathbb{R}) \rightarrow \mathbb{R}$ is a three-dimensional function we aim to learn; $Z_{u,i} = (1 - u)Z_0 + uX_i$ is the transported functional sample at time u initialized with Z_0 , which approaches X_i at $\{T_{ij}; j \in [J_i]\}$ as u increases to 1. Let \mathcal{X} be a bounded interval in \mathbb{R} that contains all values $Z_{u,i}(T_{ij})$.

We propose to restrict U within a smooth functional space to ensure smooth function generation. To achieve this, we employ spline regression to estimate the vector field. Let $\mathcal{B}_{L,q}(\mathbb{D})$ denote the L -dimensional B-spline functional space of order q , with equally spaced knots over a domain \mathbb{D} . Denote $\mathcal{B}_{L,q}(\mathbb{D}_1, \mathbb{D}_2, \mathbb{D}_3)$ as the tensor product of the spaces $\mathcal{B}_{L,q}(\mathbb{D}_1)$, $\mathcal{B}_{L,q}(\mathbb{D}_2)$, and $\mathcal{B}_{L,q}(\mathbb{D}_3)$, which consists of multivariate spline functions defined on $\mathbb{D}_1 \times \mathbb{D}_2 \times \mathbb{D}_3$. Note that the vector field $U \in \mathcal{B}_{L,4}([0, 1], \mathcal{T}, \mathcal{X})$ satisfies (10) for $q = 2$, ensuring the generation of functions from $W_2^2(\mathcal{T})$.

We consider solving the following optimization problem to estimate the vector field V :

$$\begin{aligned} \hat{V} &:= \operatorname{argmin}_{U \in \mathcal{B}_{L_V,4}([0,1], \mathcal{T}, \mathcal{X})} \{ \mathcal{L}(U) + \mathcal{J}(U) \}, \\ \text{with } \mathcal{J}(U) &= \int_{\mathcal{X}} \int_{\mathcal{T}} \int_0^1 \lambda_u \left(\frac{\partial^2 U}{\partial u^2} \right)^2 + \lambda_t \left(\frac{\partial^2 U}{\partial t^2} \right)^2 + \lambda_x \left(\frac{\partial^2 U}{\partial x^2} \right)^2 \mathrm{d}u \mathrm{d}t \mathrm{d}x, \end{aligned} \quad (20)$$

where $\mathcal{B}_{L_V,4}([0, 1], \mathcal{T}, \mathcal{X})$ denotes the space of cubic splines with L_V^3 -dimensions, $\mathcal{J}(U)$ is a penalty on the smoothness of the tensor product of spline spaces (Wood, 2006), and

λ_u , λ_t , and λ_x are tuning parameters used to control the smoothness of the vector field in different directions. To ensure the existence and uniqueness of solutions to (7) and (8) with the vector field given by \hat{V} , we restrict the class $\mathcal{B}_{L_V,4}([0, 1], \mathcal{T}, \mathcal{X})$ in (20) to contain only vector fields that satisfy the conditions of Theorem 1. This condition is imposed for technical convenience, but it is not necessary in implementation. We refer to this approach as **smooth flow matching (SFM)**.

We apply Monte Carlo sampling and discrete integration to approximate the expectation and integration to minimize (20). In detail, we first take a regularly spaced time grid $\mathcal{T}_r \subset \mathcal{T}$ such that $\cup_{i=1}^n \{T_{ij}; j \in [J_i]\} \subset \mathcal{T}_r$. Then, we generate H independent and identically distributed random functions $Z_0^{(h)}$, for $h = 1, \dots, H$, sampled on the time grid \mathcal{T}_r , where each has marginal distribution $F_{t,\text{base}}$, $t \in \mathcal{T}$. We specifically construct

$$\hat{\mathcal{L}}(U) = \frac{1}{nHF} \sum_{i=1}^n \frac{1}{J_i} \sum_{j=1}^{J_i} \sum_{h=1}^H \sum_{f=1}^F \left\{ X_i(T_{ij}) - Z_0^{(h)}(T_{ij}) - U(u_f, T_{ij}, Z_{u_f,i}^{(h)}(T_{ij})) \right\}^2, \quad (21)$$

where $Z_{u,i}^{(h)} = (1-u)Z_0^{(h)} + uX_i$ is a realization of $Z_{u,i}$, and $\{u_f; f = 1, \dots, F\}$ denotes a fixed, regularly spaced time grid in $[0, 1]$ with sufficiently large F . We then replace $\mathcal{L}(U)$ in (20) with $\hat{\mathcal{L}}(U)$ for the minimization, resulting in a standard nonparametric regression problem.

We adopt the restricted maximum likelihood (REML) method (Wood, 2011) to stably select the tuning parameters λ_u , λ_t , and λ_x in (20). This approach treats the nonparametric regression as a Bayesian regression problem, where the penalization on U corresponds to a prior distribution on U that depends on λ_u , λ_t , and λ_x . The tuning parameters are then estimated via maximum likelihood under the Bayesian framework. See Part B.5 in the Supplementary Materials for a detailed derivation.

To efficiently compute \hat{V} , we use the R package `mgcv` (Wood and Wood, 2015), which supports both optimization and REML-based tuning for (20). The smoothly estimated

vector field from (20) is then used to estimate the flow map $F_t^{-1} \circ F_{t,\text{base}}$ and its inverse $F_{t,\text{base}}^{-1} \circ F_t$ in the next section.

Remark 3 (Comparison of Smooth Flow Matching to Existing Flow-Matching Approaches).

We compare existing flow matching methods with our proposed SFM approach in Table 2.

Notably, the functional flow matching in [Kerrigan et al. \(2024\)](#) requires the transported functional sample to exactly match the target function, i.e., $Z_{1,i}(t) = X_i(t)$ for all $t \in \mathcal{T}$.

Such a strict requirement could be impractical in real applications, where each function X_i is only observed at subject-specific time points $\{T_{ij} : j \in [J_i]\}$, which vary across individuals.

In contrast, our method does not impose this condition.

Even in the fully aligned case where $\{T_{ij} : j \in [J_i]\} = \{T_j : j \in [J]\}$ for all $i = 1, \dots, n$, our approach remains distinct from existing flow matching methods ([Lipman et al., 2023](#); [Tong et al., 2024](#); [Kerrigan et al., 2024](#)). In particular, the vector field estimated in (19) is a three-dimensional function, whereas prior works typically involve estimating more complex objects: either vector fields defined on $\mathbb{R}^{J+1} \rightarrow \mathbb{R}^J$ ([Lipman et al., 2023](#); [Tong et al., 2024](#)), or operators from $\mathcal{H} \times \mathcal{T}$ to \mathcal{H} ([Kerrigan et al., 2024](#)), where \mathcal{H} is a separable Hilbert space. These are more complicated high-dimensional objects that require substantial estimation costs.

Moreover, the vector fields in [Lipman et al. \(2023\)](#); [Tong et al. \(2024\)](#); [Kerrigan et al. \(2024\)](#) are used only to construct maps from the base to the target distribution and cannot guarantee smoothness of the generated functions. In contrast, SFM facilitates both base-to-target and target-to-base transformations, while ensuring smooth generation, making it well suited for copula functional data generation.

Table 2: Comparison of flow matching methods

Name	Flow Matching (Lip- man et al., 2023; Tong et al., 2024)	Functional Matching (Kerrigan et al., 2024)	Flow Smooth	Flow Matching
Data Type	Fully observed vectors	Fully observed functions	Irregularly and sparsely observed functions	
Vector Field	Map: $\mathbb{R}^{J+1} \rightarrow \mathbb{R}^J$, J is the dimension of vectors	Map: $\mathcal{H} \times \mathcal{T} \rightarrow \mathcal{H}$, \mathcal{H} is a separable Hilbert space	Map: $\mathbb{R}^3 \rightarrow \mathbb{R}$	
Flow Model	Forward only	Forward only	Forward and backward	
Smoothness	No guarantee	No guarantee	Guaranteed	

4.2 Copula Estimation and Data Generation

In addition to the vector field V , the generation of copula functional data requires the joint distribution of the base Z_0 . In this subsection, we develop a suitable way to estimate the joint distribution based on the observed data $\{(X_i(T_{ij}), T_{ij}) : i = 1, \dots, n, j = 1, \dots, J_i\}$. We begin by demonstrating the Gaussian copula process case, i.e., setting $F_{t,\text{base}} = \Phi$ for all $t \in \mathcal{T}$, and then extend the methodology to the Student- t copula and more general copula settings in Parts B.1 and B.2 of the Supplementary Materials, respectively.

To generate the base process, we require the estimation of the latent correlation function ρ . We achieve this by the following three-step procedure.

- Based on Theorem 1 (b), we define $\hat{\psi}_{1,t}(z)$ as the solution to the differential equation:

$$\frac{\partial \hat{\psi}_{u,t}(z)}{\partial u} = -\hat{V}(1-u, t, \hat{\psi}_{u,t}(z)) \quad \text{subject to} \quad \hat{\psi}_{0,t}(z) = z, \quad (22)$$

where \hat{V} is obtained from (20). Then, $\hat{\psi}_{1,t}$ is an estimate of $\Phi^{-1} \circ F_t$. Accordingly, we compute

$$G_i(T_{ij_1}, T_{ij_2}) = \hat{\psi}_{1,T_{ij_1}}(X_i(T_{ij_1})) \cdot \hat{\psi}_{1,T_{ij_2}}(X_i(T_{ij_2})) \quad (23)$$

for each i, j_1, j_2 , serving as an empirical estimate of $\rho(T_{ij_1}, T_{ij_2})$ in (3).

- Second, we propose to apply surface smoothing methods with penalized bivariate spline on $\{G_i(T_{ij_1}, T_{ij_2}); i = 1, \dots, n, j_1, j_2 = 1, \dots, J_i\}$ to estimate the correlation function ρ :

$$\hat{\rho} = \operatorname{argmin}_{f \in \mathcal{B}_{L_\rho, 4}(\mathcal{T}, \mathcal{T})} \left[\frac{1}{n} \sum_{i=1}^n \frac{1}{J_i^2} \sum_{j_1, j_2=1}^{J_i} \{G_i(T_{ij_1}, T_{ij_2}) - f(T_{ij_1}, T_{ij_2})\}^2 + \mathcal{J}(f) \right], \quad (24)$$

where $\mathcal{J}(f) = \int_{\mathcal{T}} \int_{\mathcal{T}} \left\{ \lambda_1 \left(\frac{\partial^2 f(t_1, t_2)}{\partial t_1^2} \right)^2 + \lambda_2 \left(\frac{\partial^2 f(t_1, t_2)}{\partial t_2^2} \right)^2 \right\} dt_1 dt_2$ is a penalization term to control the smoothness of $\hat{\rho}$. We adopt a similar strategy as in (20) for optimizing (24) and tuning the parameters λ_1 and λ_2 using the REML method. The estimated latent correlation function then guarantees the generation of smooth Gaussian processes from $W_2^2(\mathcal{T})$, as ensured by Example 2. To guarantee that $\hat{\rho}$ is a valid covariance function, we restrict the class $\mathcal{B}_{L_\rho, 4}$ to contain only positive-definite kernels. In practice, this can be approximated by first ignoring the positive-definiteness constraint in the optimization (24), and then applying the nearest positive definite (NPD) approximation (Higham, 2002) to the estimated kernel $\hat{\rho}$ on a chosen time grid.

- Third, given the estimated vector field and latent correlation function, we generate \tilde{Z}_0 as a mean-zero Gaussian process with covariance $\hat{\rho}$, and then apply the transformation $\widehat{F_t^{-1} \circ \Phi}(\tilde{Z}_0(t))$, $t \in \mathcal{T}$, to produce new functional samples. Here, the flow map $\widehat{F_t^{-1} \circ \Phi}(x)$ is the solution $\hat{\phi}_{1,t}(x)$ of the differential equation.

$$\frac{\partial \hat{\phi}_{u,t}(x)}{\partial u} = \hat{V}(u, t, \hat{\phi}_{u,t}(x)), \quad \text{subject to} \quad \hat{\phi}_{0,t}(x) = x, \quad (25)$$

in accordance with Definition 2.

We summarize the complete data generation procedure of SFM for Gaussian copula processes in Algorithm 1, incorporating the estimated vector fields and latent correlation

functions. The numerical solutions required for computing $G_i(T_{ij_1}, T_{ij_2})$ and for generating functional data are implemented using the Runge–Kutta method, as detailed in Proposition S1 of the Supplementary Materials.

Algorithm 1 Smooth Flow Matching for Gaussian Copula Processes

- 1: **Input:** Observed data $\{(X_i(T_{ij}), T_{ij}); i = 1, \dots, n, j = 1, \dots, J_i\}$, number of samples H for estimation, and number of samples M for generation. A regularly spaced time grid \mathcal{T}_r such that $\cup_{i=1}^n \{T_{ij}; j \in [J_i]\} \subset \mathcal{T}_r$.
- 2: Generate H independent and identical mean-zero Gaussian processes, $Z_0^{(h)}, h = 1, \dots, H$, sampled at the time grid \mathcal{T}_r , with the covariance function being $\mathbb{I}(t = s)$.
- 3: Obtain the vector field \hat{V} from $\hat{V} := \operatorname{argmin}_{U \in \mathcal{B}_{LV,4}([0,1], \mathcal{T}, \mathcal{X})} \{\hat{\mathcal{L}}(U) + \mathcal{J}(U)\}$.
- 4: Calculate $G_i(T_{ij_1}, T_{ij_2}) = \hat{\psi}_{1,T_{ij_1}}(X_i(T_{ij_1})) \cdot \hat{\psi}_{1,T_{ij_2}}(X_i(T_{ij_2}))$, where $\hat{\psi}_{1,t}(z)$ is the solution of
$$\frac{\partial \hat{\psi}_{u,t}(z)}{\partial u} = -\hat{V}(1-u, t, \hat{\psi}_{u,t}(z)), \text{ subject to } \hat{\psi}_{0,t}(z) = z.$$
- 5: Apply surface smoothing (24) on $\{G_i(T_{ij_1}, T_{ij_2}); i = 1, \dots, n, j_1, j_2 = 1, \dots, J_i\}$ to obtain $\hat{\rho}(t, s)$. Employ the NPD approximation for the kernel $\hat{\rho}$ on $\mathcal{T}_r \times \mathcal{T}_r$.
- 6: Regenerate M independent and identical mean-zero Gaussian processes, $\tilde{X}_0^{(l)}, l = 1, \dots, L$, sampled at the time grid \mathcal{T}_r , with the covariance function being the NPD approximation of $\hat{\rho}(t, s)$.
- 7: For $l = 1, \dots, L$ and $t \in \mathcal{T}_r$, solve the equation $\frac{\partial \tilde{X}_u^{(l)}(t)}{\partial u} = \hat{V}(u, t, \tilde{X}_u^{(l)}(t))$ given the initial value $\tilde{X}_0^{(l)}(t)$, obtaining $\tilde{X}_1^{(l)}(t)$ for each $t \in \mathcal{T}_r$.
- 8: **Output:** synthetic functions $\tilde{X}_1^{(l)}(t), t \in \mathcal{T}_r$ and $l = 1, \dots, M$.

Remark 4 (Smooth Flow Matching for Noisy Data). When we collect Y_{ij} rather than its noiseless observations $X_i(T_{ij})$, we can apply smoothing splines (Gu, 2013) to the paired observations $\{(T_{ij}, Y_{ij}); j = 1, \dots, J_i\}$ for each i , yielding smoothed trajectories \hat{X}_i . This process removes noise from the observations by leveraging the smoothness of the underlying curves. The denoised values $(\{\hat{X}_i(T_{ij}), T_{ij}\}; i = 1, \dots, n, j = 1, \dots, J_i)$ are then used as input for SFM in Algorithms 1.

4.3 Consistency of Smooth Flow Matching

In this subsection, we establish the statistical consistency for the proposed smooth flow matching. Suppose that the time points $\{T_{ij}; i = 1, \dots, n, j = 1, \dots, J_i\}$ and the functional observations $\{X_i; i = 1, \dots, n\}$ are independent. The number of observations J_i , for $i = 1, \dots, n$, is deterministic and bounded. We also introduce the following assumptions.

Assumption 1. The time points $\{T_{ij}; i = 1, \dots, n, j = 1, \dots, J_i\}$ are independently drawn from a density function p_T , where p_T is positive and bounded away from zero on \mathcal{T} .

Assumption 2. X_i s are independent and identically distributed Gaussian copula processes with latent correlation function ρ , where $\mathbb{E}\|X_i\|^4$ is bounded by a constant and $\rho \in \mathcal{W}_2^2(\mathcal{T} \times \mathcal{T})$ has second-order derivatives with bounded L^2 -norm.

Assumption 3. Z_0 in (19) satisfies $\mathbb{E}\|Z_0\|^4$ is bounded by a constant. For $u \in [0, 1]$ and $t \in \mathcal{T}$, $Z_{u,i}(t) = (1 - u)Z_0(t) + uX_i(t)$ has a density $p_{Z_{u,i}(t)}$ that is positive and bounded over its support.

Assumption 4. The true vector field V in (18) is unique and belongs to $\mathcal{W}_2^2([0, 1] \times \mathcal{T} \times \mathcal{X})$. Besides, V satisfies the conditions in Theorem 1 and its second-order derivatives have bounded L^2 -norm.

To quantify the discrepancy between the true distribution of functional data X and the generated functional data \tilde{X} by SFM, we use the Wasserstein distance:

$$W_2(X, \tilde{X}) = \inf_{\gamma \in \Gamma(\nu, \tilde{\nu})} \left(\int \|X - \tilde{X}\|^2 d\gamma(X, \tilde{X}) \right)^{1/2}, \quad (26)$$

where ν and $\tilde{\nu}$ are the distributions of X and \tilde{X} , respectively, and $\Gamma(\nu, \tilde{\nu})$ is the set of all couplings between ν and $\tilde{\nu}$.

Under the above conditions, we have the following theorem.

Theorem 4 (Consistency of the Estimated Vector Field, Latent Correlation Function, and Generated Functional Data). Suppose that Assumptions 1–4 hold. Let the tuning parameters in estimating vector field $L_V, \lambda_u, \lambda_t, \lambda_x$ in (20) satisfy $L_V \rightarrow \infty$ and $L_V = o(n^{1/3})$, and $\max\{\lambda_u, \lambda_t, \lambda_x\} = o(1)$, as $n \rightarrow \infty$. Meanwhile, let the parameters in estimating latent correlation function $L_\rho, \lambda_1, \lambda_2$ in (24) satisfy $L_\rho \rightarrow \infty$, $L_\rho = o(n^{1/2})$, and $\max\{\lambda_1, \lambda_2\} = o(1)$, as $n \rightarrow \infty$. Then the estimators \hat{V} and $\hat{\rho}$ are consistent:

$$\|V - \hat{V}\| \xrightarrow{p} 0 \quad \text{and} \quad \|\rho - \hat{\rho}\| \xrightarrow{p} 0, \quad \text{as } n \rightarrow \infty.$$

Consequently, the Wasserstein distance between X and \tilde{X} converges to zero in probability:

$$W_2(X, \tilde{X}) \xrightarrow{p} 0, \quad \text{as } n \rightarrow \infty.$$

Note that Theorem 4 does not require $\min_{i=1, \dots, n} J_i \rightarrow \infty$ as $n \rightarrow \infty$. Consequently, SFM is applicable to practical settings where the functional data are irregularly and sparsely observed.

5 Simulation Studies

In this section, we evaluate the performance of the proposed SFM method for generating smooth functional data. The presented result of each setting is based on 100 replications.

Data Generation We consider both Gaussian and non-Gaussian settings.

- **Gaussian Case:** We generate sparsely observed functional data using the KL expansion:

$$X_i(T_{ij}) = \mu(T_{ij}) + \sum_{k=1}^K \xi_{ik} \psi_k(T_{ij}), \quad i = 1, \dots, n; \quad j = 1, \dots, J_i,$$

where $\mu(t)$ is a fixed mean function constructed as a linear combination of degree-4 B-spline basis functions with coefficients independently drawn from $\mathcal{N}(0, 1)$; $\psi_k, k =$

$1, \dots, K$, are the first $K = 4$ non-constant Fourier basis functions; $\xi_{ik} \sim \mathcal{N}(0, \sigma_k^2)$, with $\sigma_k = \|\mu\| \cdot \exp((5-k)/5)/2$; J_i is randomly sampled from either $\{2, \dots, 6\}$ or $\{6, \dots, 10\}$; the time points T_{ij} are drawn independently from a uniform distribution over an equally spaced 50-point grid on $[0, 1]$.

- **Non-Gaussian Case:** We transform the latent Gaussian process above using a Gamma copula transformation:

$$X_i(T_{ij}) = \Gamma^{-1} \left(\Phi_{T_{ij}} \left(\mu(T_{ij}) + \sum_{k=1}^K \xi_{ik} \psi_k(T_{ij}) \right); 0.5, 1 \right),$$

where Φ_t is the distribution function of the latent Gaussian variable at time t , and $\Gamma^{-1}(\cdot; 0.5, 1)$ is the quantile function of the Gamma distribution with shape 0.5 and rate 1. All other components $(\mu, \xi_{ik}, \psi_k, K, T_{ij}, J_i)$ are defined as in the Gaussian case.

We compare SFM with four baseline methods. DSM (Denoising Score Matching) is based on score-based diffusion models in function space (Lim et al., 2023), using neural operator techniques to estimate score functions for functional generation. FM (Flow Matching) is a flow-based approach that employs neural operators to estimate functional vector fields (Kerrigan et al., 2024). GP (Gaussian Process Sampling) is a traditional functional data analysis method; it estimates the mean and covariance functions using smoothing techniques (Yao et al., 2005; Hsing and Eubank, 2015), then samples functions under the assumption of a Gaussian process prior. Finally, KL (KL Expansion with FPCA) estimates eigenfunctions and eigenvalues via functional principal component analysis (FPCA), and generates new functions by sampling Gaussian scores scaled by the estimated eigenvalues (Yao et al., 2005; Hsing and Eubank, 2015).

The DSM and FM methods are implemented in Python, while GP, KL, and SFM are implemented in R. SFM is implemented using Algorithm 1, adopting smooth estimation

(20) for the vector field using the tensor-product spline $\mathcal{B}_{6,4}([0, 1], \mathcal{T}, \mathcal{X})$. For modeling the scores or vector fields in DSM and FM, we employ the Fourier Neural Operator (FNO; [Li et al., 2020](#)) architecture for modelling, with 20 Fourier modes, 3 layers, and a channel width of 30. Both are trained for 5000 epochs. Because DSM and FM require fully observed functions, we first interpolate each sparse trajectory using cubic splines on the 50-point time grid before training and sampling. All experiments are conducted on a high-performance machine with 40 cores and 208 GB of RAM.

Evaluation Measure We adopt the Wasserstein distance (26) to quantify the discrepancy between the true distribution of functional data and that of the generated functional data. We draw 100 samples from each distribution and compute the empirical Wasserstein distance using the `transport` package in R ([Gottschlich and Schuhmacher, 2014](#)).

Results Figure 2 summarizes the results across different combinations of sample sizes n and sparsity levels J_i . It reports both the Wasserstein distance between the true and generated distributions from replicated simulations, and the average computation time required to estimate the data generator for each method.

For the Gaussian case, SFM performs comparably to GP and KL, even though it does not explicitly assume Gaussianity in its modeling procedure. In contrast, DSM and FM yield the poorest performance when the observed functional data are relatively sparse, likely due to the additional uncertainty introduced by the interpolation step required before training.

A similar pattern holds in the non-Gaussian (Gamma) case: DSM and FM continue to underperform, while GP and KL now exhibit the largest errors, reflecting their strong reliance on the Gaussian assumption, which is violated in this setting.

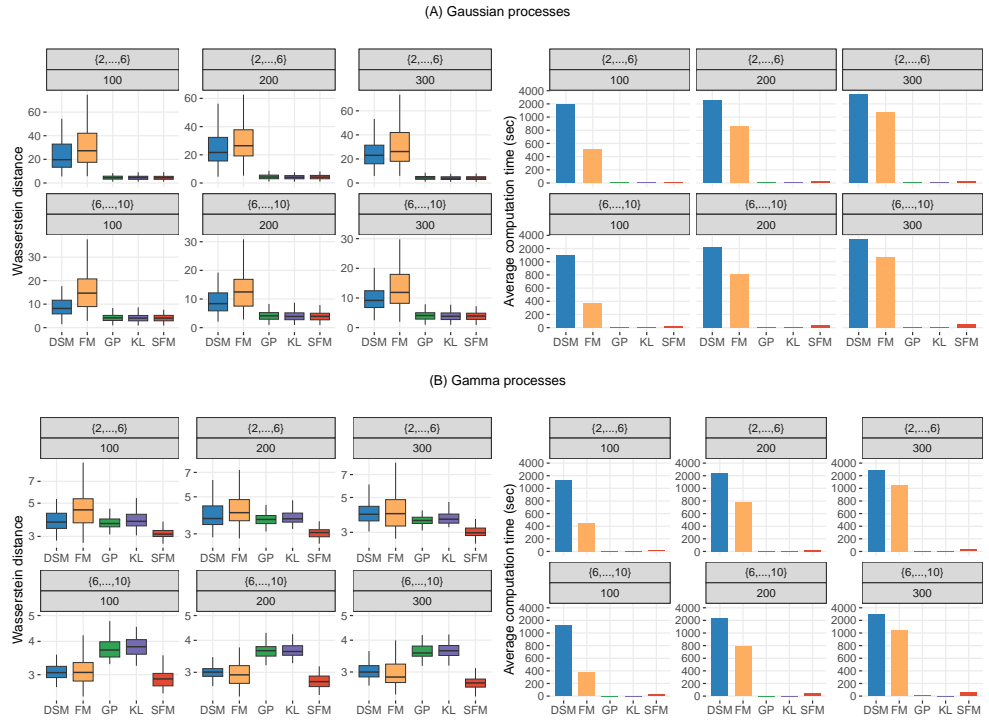


Figure 2: Left panel: Box plots for Wasserstein distances from 100 simulation replications under varying sample sizes n (subtitle) numbers of observed time points J_i (main title). Right panel: average computation times.

Across both scenarios, SFM consistently produces the most accurate or at least competitive functional samples relative to all other methods. In addition, SFM is substantially more computationally efficient than DSM and FM, as it bypasses the need for neural operator estimation during training.

We illustrate the functional data generated by different methods in Figure 3. DSM and FM often produce non-smooth functions across settings, likely due to the absence of explicit smoothness constraints in their generative models. GP and KL yield visually plausible samples in the Gaussian case; however, in the Gamma case, their outputs frequently take negative values, contradicting the true data's positive support. In contrast, our proposed SFM method generates smooth functional data that largely align with the correct support

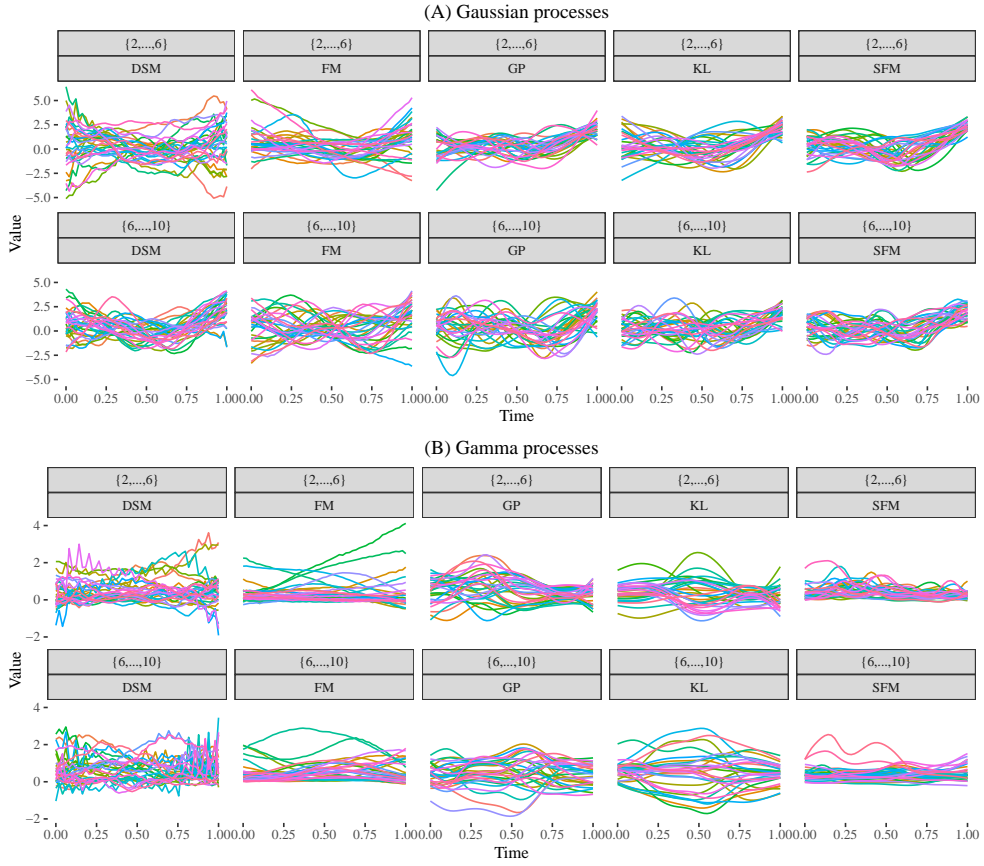


Figure 3: Illustration of generated functional data for different observed time points (main title) and different methods (sub-title). The sample sizes n are set to 100 for the generation.

in both the Gaussian and Gamma settings.

To further evaluate generation quality, we compute the mean squared error (MSE) between ground-truth targets—namely the mean function (MF), the first two eigenfunctions (EF1, EF2), and the median function (MDF)—and their corresponding estimates from the generated data. The median function is defined pointwise as the median of the random variable $X(t)$, for $t \in \mathcal{T}$. In the Gaussian case, we report MSEs for MF, EF1, and EF2; in the Gamma case, we additionally report MDF. As a baseline, we also include an oracle method that applies FPCA (Hsing and Eubank, 2015) directly to the observed training data to estimate MF, EF1, and EF2.

The results, summarized in Table S1 of the Supplementary Materials, show that SFM, GP, and KL achieve comparable performance in recovering the mean and leading eigenfunctions, and they achieve better performance than DSM and FM. Compared to GP and KL, SFM provides a more accurate estimation of the median trend in the Gamma setting, highlighting its advantage in capturing features beyond second-order moments—something GP and KL are not designed to do. Note that in both cases, SFM performs near or on par with the oracle method in estimating both the mean function and the eigenfunctions. These results collectively show the robustness and flexibility of SFM in handling complex and heavy-tailed functional data.

Furthermore, we provide a sensitivity analysis to evaluate the impact of measurement noise on SFM in Part C.2 of the Supplementary Materials. To this end, we simulate noisy functional data by adding Gaussian noise. SFM is then applied both directly to the noisy data and to denoised data obtained from Remark 4, and we evaluate synthetic data from noisy and denoised data based on Wasserstein distances. Our results indicate that the performance of SFM slightly deteriorates as the noise level increases. In contrast, applying denoising to the data prior to generation improves the performance of SFM, making it less sensitive to the added noise.

6 Real Data Analysis

In this section, we apply the proposed SFM method to the MIMIC-IV electronic health records (EHR) database ([Johnson et al., 2024](#)), which contains de-identified ICU records from the Beth Israel Deaconess Medical Center collected between 2008 and 2019. The dataset includes longitudinal clinical measurements recorded during ICU stays, offering valuable insights into the temporal dynamics of patient health. Such data are critical

for monitoring clinical progression, informing medical decisions, and developing predictive models in healthcare.

Our goal is to synthesize realistic surrogate patient trajectories that preserve the underlying temporal patterns of the observed data. We compare the performance of SFM with two baseline methods, DSM and FM, as introduced in the simulation section. DSM and FM were implemented in `Python`, while SFM was implemented in `R`. All computations were conducted on a server with 40 CPU cores and 208 GB of RAM.

We focus on ICU patients who were eventually discharged. To mitigate the influence of outlier values, we remove the top 1% of measurements across all patient trajectories for each clinical feature. Each patient’s data are then treated as a random function over a time domain, where time zero represents the ICU admission. The endpoint of the time domain is selected such that 80% of all patient observations fall within this interval. We retain patient-level trajectories with at least four time points. To reduce observational noise, we apply smoothing splines (Gu, 2013) to each patient’s functional data, consistent with the denoising step in Remark 4. Due to substantial variability in measurement times across patients, we obtain irregularly sampled functional data for each feature after the preprocessing.

Our analysis focuses on three clinical features: arterial blood pressure, respiratory rate, and heart rate. The corresponding numbers of patients are $n = 256$, 1446, and 1446, respectively. The preprocessed, denoised functional data for these features are illustrated in Figure 4 (A).

We apply SFM with both Gaussian and Student- t bases (Algorithms 1 and Algorithms S1 in the Supplementary Materials) to each clinical feature in order to synthesize new functional samples. To assess performance, we compare SFM to DSM and FM,

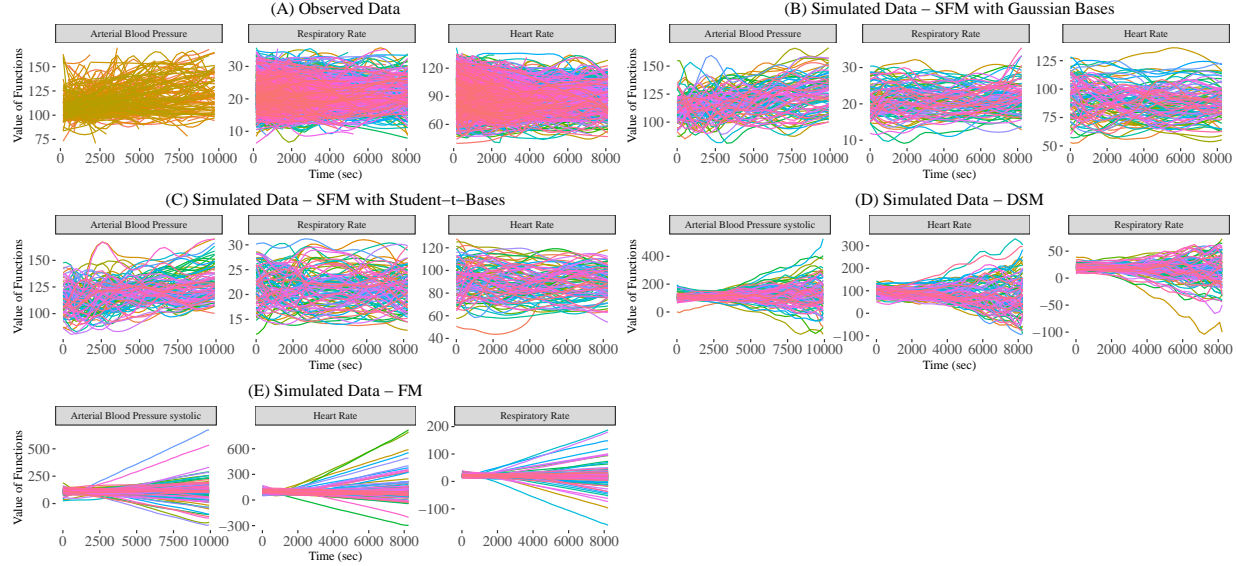


Figure 4: **(A)**: Irregularly observed functional data for each clinical feature; **(B)**: Synthetic functional data using SFM with Gaussian bases; **(C)**: Synthetic functional data using SFM with Student- t bases; **(D)**: Synthetic functional data using DSM; **(E)**: Synthetic functional data using FM.

using the same neural network architecture as in the simulation study. Since DSM and FM require fully observed functional trajectories, we impute missing values by applying smoothing splines, as described previously, over a fixed evaluation grid \mathcal{T}_r . This grid consists of 31 equally spaced time points spanning the observed time domain of each clinical feature, approximately covering all time points at which any patient was measured.

Figure 4 (B) – (E) displays synthetic functional samples generated by SFM, as well as by DSM and FM, evaluated on \mathcal{T}_r . For each method and feature, we generate 100 synthetic samples. We also report the computational training times for SFM, DSM, and FM in Table 3. The results show that SFM achieves significantly shorter training time compared to DSM and FM, highlighting its computational efficiency.

Table 3: Computational time for training the data generator of different methods.

Time (sec)	SFM (Gaussian base)	SFM (Student- t base)	DSM	FM
Arterial blood pressure	25.92	44.52	1575.72	332.65
Respiratory rate	194.03	247.40	4220.99	1663.85
Heart rate	194.62	248.09	4311.92	1684.52

In Figure 4, we observe that the functional samples generated by DSM and FM differ substantially from the observed data. This discrepancy is largely attributable to the irregular sampling in the original dataset, which results in a high proportion of missing values that must be imputed prior to model training. The imputation process not only denoises the observed values but also extrapolates values at time points outside the range of actual observations for some patients. Such extrapolation can introduce considerable error—spline smoothing often imputes out-of-sample regions as nearly linear, which may poorly capture the true underlying dynamics and consequently degrade the quality of the synthesized samples.

Evaluation on Dimension Reduction To evaluate the quality of the synthesized data, we estimate the mean function and the first two eigenfunctions from both the observed and the synthesized functional data. For each clinical feature, the synthetic sample size is set to match the number of patients. Estimation is carried out using smoothing-based functional data analysis methods (Yao et al., 2005; Hsing and Eubank, 2015), consistent with the procedures used in the simulation study. The results are presented in Figure 5 (A).

We find that the mean and eigenfunctions estimated from DSM- and FM-generated samples differ substantially from those of the observed data. In contrast, the estimates derived from SFM-synthesized data closely match the corresponding patterns from the real data, indicating SFM’s ability to recover key temporal dynamics in EHR trajectories.

Furthermore, the results from SFM are nearly identical across different base distributions (Gaussian and Student- t), suggesting that the dominant functional patterns are robust to the choice of bases.

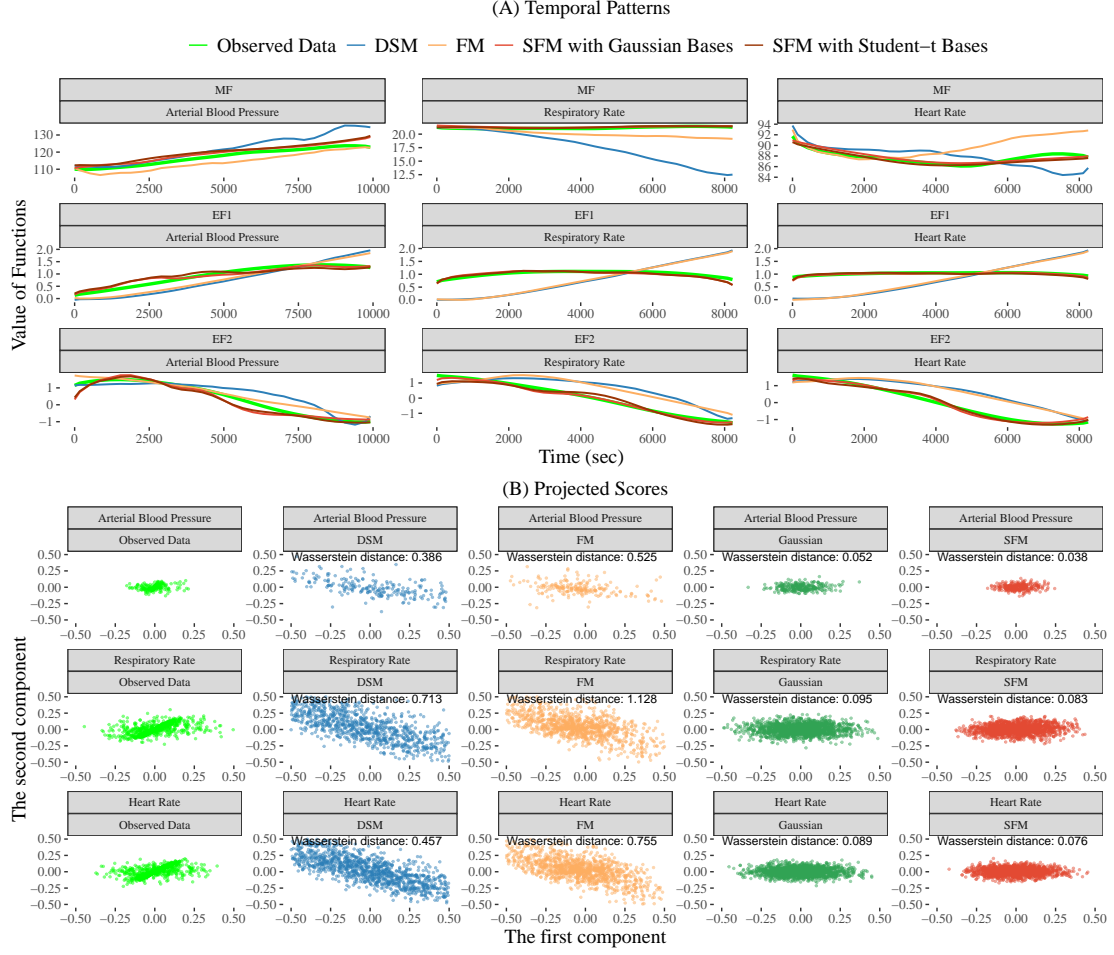


Figure 5: (A): The estimated mean function (MF) and the first two eigenfunctions (EF 1 and 2) of the observed functional data and the synthesized functional data. (B): The projected scores for the observed data and the synthetic data, as well as those generated by the Gaussian method. The Wasserstein distances for the last four columns are computed between their corresponding samples and those of the observed data.

To further assess performance, we project both the observed and synthesized functional data onto the eigenfunctions estimated from the observed data (green lines labeled EF1 and

EF2 in Figure 5 (A)). For the synthesized data, projections are computed via numerical integration over the fixed grid \mathcal{T}_r , yielding two-dimensional score vectors for each subject. To handle irregular sampling in the observed data, we apply a shrinkage approach for score estimation, following [Yao et al. \(2003\)](#). These scores represent dominant modes of variation in the data, with variances determined by the associated eigenvalues.

As an additional baseline, we include a Gaussian score-generating method that samples each score dimension independently from a mean-zero Gaussian distribution, with variances set to the corresponding eigenvalues estimated from the observed data ([Yao et al., 2005](#)). The score distributions from the observed data, SFM (Gaussian base), DSM, FM, and the Gaussian-based method are shown in Figure 5 (B), with synthetic sample sizes again matched to the observed data.

We observe that the scores from DSM and FM deviate significantly from those of the observed data, reflecting poor alignment with the underlying data structure. In contrast, scores from SFM and the Gaussian-based method both exhibit patterns similar to those of the observed data, with SFM showing even closer alignment. This suggests that SFM captures higher-order or non-Gaussian characteristics present in the EHR data, beyond what is captured by the purely Gaussian score generation approach.

Evaluation on Data Prediction To assess the practical utility of the synthesized data, we consider a one-step-ahead prediction task:

$$X_i(T_{j+1}) = f(X_i(T_j), T_j) + \tau_{ij}, \quad i = 1, \dots, n, \quad j = 1, \dots, 30, \quad (27)$$

where $X_i(T_j)$ denotes the synthesized or observed denoised functional data for subject i at time T_j , $\mathcal{T}_r = \{T_j; j = 1, \dots, 31\}$ is an equally spaced time grid, τ_{ij} are mean-zero noise terms, and $f(\cdot, t)$ is the unknown prediction function at time t . We compare the

prediction functions estimated from synthesized and observed functional data to evaluate the predictive utility of each dataset. The estimation can be performed using nonparametric regression based on (27); see Part B.6 in the Supplementary Materials for a demonstration.

We estimate f from the observed data and from synthetic datasets generated by SFM, FM, and DSM. For comparison, we also include synthetic datasets produced by the GP and KL methods described in the simulation section. Predictive performance is evaluated using the g -step-ahead relative prediction error on the observed validation data:

$$\text{Error}_g = \sqrt{\sum_{i \in \mathcal{V}} \sum_{j=1}^{J-g} \left\{ X_i(T_{j+g}) - \hat{f}_{T_j}^g(X_i(T_j)) \right\}^2 \cdot \mathcal{I}_{T_j, T_{j+g}}(X_i)},$$

where $\mathcal{I}_{T_j, T_{j+1}}(X_i) = 1$ if X_i is observed at both T_j and T_{j+1} , and 0 otherwise, and $\hat{f}_{T_j}^g$ is the recursively defined g -step-ahead predictor, which is $\hat{f}_{T_j}^g(X_i(T_j)) = \hat{f}(\hat{f}(\cdots \hat{f}(X_i(T_j), T_j) \cdots, T_{j+g-2}), T_{j+g-1})$, and \mathcal{V} indexes the validation set.

For the observed data, we randomly split the original dataset into training (\mathcal{E}) and validation (\mathcal{V}) sets of equal size. We train \hat{f} on \mathcal{E} and evaluate performance on \mathcal{V} . For the generative methods, we synthesize a dataset \mathcal{E}_{syn} matching the size of \mathcal{E} , train \hat{f} on \mathcal{E}_{syn} , and evaluate performance on \mathcal{V} . We repeat this process 200 times and report average Error_g for different prediction horizons g (Figure 6).

Figure 6 shows SFM achieves the lowest Error_g among all generative methods, indicating that it produces synthetic data with superior predictive power. Notably, its prediction error is close to that of the observed data, and even lower when the sample size is small (e.g., Arterial Blood Pressure with $n = 256$, compared to $n = 1446$ for other features). This suggests that SFM generates reliable, densely sampled functional data, which can reduce prediction uncertainty, especially in settings with limited or irregularly sampled observations.

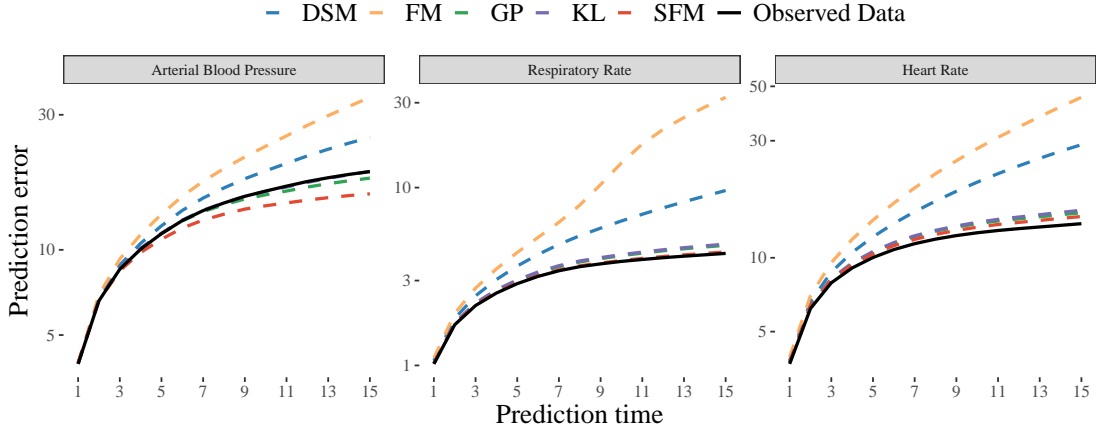


Figure 6: Prediction errors of different methods across various prediction horizons g .

7 Discussions

In this article, we introduce a novel smooth flow matching (SFM) method tailored for generating new functional samples from irregularly observed functional data. Our approach proposes a copula-based semiparametric framework that learns general marginal distributions of random functions while enforcing smoothness in the synthesized samples. It offers an interpretable, flexible, and computationally efficient data generator that does not rely on assumptions such as Gaussianity, low-rank structure, or dense and regular observations, nor does it require computationally intensive operator learning—requirements often imposed by existing methods. Simulation studies demonstrate the superior performance of SFM in terms of the quality of generated samples, computational efficiency, and its ability to capture the rich distributional characteristics of random functions.

We then apply SFM to real-world EHR longitudinal data that consist of irregularly observed functional data. The SFM-synthetic data successfully recover the dominant temporal patterns and key distributional features across patients of the original EHR data. In addition, predictive models trained on SFM-generated data outperform those trained on

data from alternative methods and perform comparably to models trained on the original data. This demonstrates the advantage of SFM in producing high-quality surrogate data that reflect the predictive power of the EHR data.

The current work has some limitations. First, we do not provide the convergence rate of SFM for data generation when the functional data are discretely observed. Similar to existing works (Cai and Yuan, 2011; Hsing and Eubank, 2015), discreteness may lead to a transition in convergence properties between settings where observational times are sparsely versus densely observed. This transition complicates the analysis of the regression problem with the loss (19) for vector field estimation, where the time variable not only serves as an explicit argument of the regression function but is also embedded within another dimension. Secondly, this article mainly focuses on univariate functional data generation based on irregular observations. Extending the SFM framework to irregularly observed multivariate functional data is also meaningful in many real-world settings, such as EHR data (Johnson et al., 2024), spatio-temporal data (Tan et al., 2024a), and epidemiological data (Luo et al., 2025), where capturing interdependencies among random functions is helpful. We leave them as future work for further investigation.

References

Butcher, J. C. (1996). A history of runge-kutta methods. *Applied numerical mathematics*, 20(3):247–260.

Cai, T. T. and Yuan, M. (2011). Optimal estimation of the mean function based on discretely sampled functional data: Phase transition. *The Annals of Statistics*, 39(5):2330–2355.

Carroll, C., Bhattacharjee, S., Chen, Y., Dubey, P., Fan, J., Gajardo, Á., Zhou, X.,

Müller, H.-G., and Wang, J.-L. (2020). Time dynamics of covid-19. *Scientific reports*, 10(1):21040.

Chen, R. T., Rubanova, Y., Bettencourt, J., and Duvenaud, D. K. (2018). Neural ordinary differential equations. *Advances in neural information processing systems*, 31.

Chiou, J.-M. and Li, P.-L. (2007). Functional clustering and identifying substructures of longitudinal data. *Journal of the Royal Statistical Society Series B: Statistical Methodology*, 69(4):679–699.

de Boor, C. and DeVore, R. (1983). Approximation by smooth multivariate splines. *Transactions of the American Mathematical Society*, 276(2):775–788.

Demarta, S. and McNeil, A. J. (2005). The t copula and related copulas. *International statistical review*, 73(1):111–129.

Franzese, G., Corallo, G., Rossi, S., Heinonen, M., Filippone, M., and Michiardi, P. (2023). Continuous-time functional diffusion processes. *Advances in Neural Information Processing Systems*, 36:37370–37400.

Golda, A., Mekonen, K., Pandey, A., Singh, A., Hassija, V., Chamola, V., and Sikdar, B. (2024). Privacy and security concerns in generative ai: a comprehensive survey. *IEEE Access*, 12:48126–48144.

Gonzales, A., Guruswamy, G., and Smith, S. R. (2023). Synthetic data in health care: A narrative review. *PLOS Digital Health*, 2(1):e0000082.

Gottschlich, C. and Schuhmacher, D. (2014). The shortlist method for fast computation

of the earth mover’s distance and finding optimal solutions to transportation problems.

PloS one, 9(10):e110214.

Gu, C. (2013). *Smoothing spline ANOVA models*, volume 297. Springer.

Happ, C. and Greven, S. (2018). Multivariate functional principal component analysis for data observed on different (dimensional) domains. *Journal of the American Statistical Association*, 113(522):649–659.

Henderson, I. (2024). Sobolev regularity of gaussian random fields. *Journal of Functional Analysis*, 286(3):110241.

Higham, N. J. (2002). Computing the nearest correlation matrix—a problem from finance. *IMA journal of Numerical Analysis*, 22(3):329–343.

Hsing, T. and Eubank, R. (2015). *Theoretical foundations of functional data analysis, with an introduction to linear operators*, volume 997. John Wiley & Sons.

James, G. M., Hastie, T. J., and Sugar, C. A. (2000). Principal component models for sparse functional data. *Biometrika*, 87(3):587–602.

Jaworski, P., Durante, F., Hrdle, W. K., and Rychlik, T. (2010). *Copula theory and its applications*, volume 198. Springer.

Johnson, A., Bulgarelli, L., Pollard, T., Gow, B., Moody, B., Horng, S., Celi, L. A., and Mark, R. (2024). “mimic-iv” (version 3.0). *PhysioNet*.

Kerrigan, G., Ley, J., and Smyth, P. (2023). Diffusion generative models in infinite dimensions. In *International Conference on Artificial Intelligence and Statistics*, pages 9538–9563. PMLR.

Kerrigan, G., Migliorini, G., and Smyth, P. (2024). Functional flow matching. In *International Conference on Artificial Intelligence and Statistics*, pages 3934–3942. PMLR.

LeCun, Y., Bengio, Y., and Hinton, G. (2015). Deep learning. *nature*, 521(7553):436–444.

Li, Z., Kovachki, N., Azizzadenesheli, K., Liu, B., Bhattacharya, K., Stuart, A., and Anandkumar, A. (2020). Fourier neural operator for parametric partial differential equations. *arXiv preprint arXiv:2010.08895*.

Lim, J. H., Kovachki, N. B., Baptista, R., Beckham, C., Azizzadenesheli, K., Kossaifi, J., Voleti, V., Song, J., Kreis, K., Kautz, J., et al. (2023). Score-based diffusion models in function space. *arXiv preprint arXiv:2302.07400*.

Lipman, Y., Chen, R. T. Q., Ben-Hamu, H., Nickel, M., and Le, M. (2023). Flow matching for generative modeling. In *The Eleventh International Conference on Learning Representations*.

Liu, X., Gong, C., and Liu, Q. (2022). Flow straight and fast: Learning to generate and transfer data with rectified flow. *arXiv preprint arXiv:2209.03003*.

Luo, F., Tan, J., Zhang, D., Huang, H., and Shen, Y. (2025). Functional clustering for longitudinal associations between social determinants of health and stroke mortality in the us. *The Annals of Applied Statistics*, 19(1):798–820.

Mallasto, A. and Feragen, A. (2017). Learning from uncertain curves: The 2-wasserstein metric for gaussian processes. *Advances in Neural Information Processing Systems*, 30.

Nie, Y., Yang, Y., Wang, L., and Cao, J. (2022). Recovering the underlying trajectory from sparse and irregular longitudinal data. *Canadian Journal of Statistics*, 50(1):122–141.

Ohalete, N. C., Ayo-Farai, O., Onwumere, C., Maduka, C. P., and Olorunsogo, T. O. (2024). Functional data analysis in health informatics: A comparative review of developments and applications in the usa and africa. *World Journal of Advanced Research and Reviews*, 21(1):1097–1114.

Papamakarios, G., Nalisnick, E., Rezende, D. J., Mohamed, S., and Lakshminarayanan, B. (2021). Normalizing flows for probabilistic modeling and inference. *Journal of Machine Learning Research*, 22(57):1–64.

Ramsay, J. and Hooker, G. (2017). Dynamic data analysis. *Springer New York, New York, NY*. doi, 10:978–1.

Ramsay, J. and Silvermann, B. (2005). *Functional data analysis. springer series in statistics*. Wiley Online Library.

Shen, X., Liu, Y., and Shen, R. (2023). Boosting data analytics with synthetic volume expansion. *arXiv preprint arXiv:2310.17848*.

Shi, P., Martino, C., Han, R., Janssen, S., Buck, G., Serrano, M., Owzar, K., Knight, R., Shenhav, L., and Zhang, A. R. (2024). Tempted: time-informed dimensionality reduction for longitudinal microbiome studies. *Genome Biology*, 25(1):317.

Song, Y. and Ermon, S. (2019). Generative modeling by estimating gradients of the data distribution. *Advances in neural information processing systems*, 32.

Staicu, A.-M., Crainiceanu, C. M., Reich, D. S., and Ruppert, D. (2012). Modeling functional data with spatially heterogeneous shape characteristics. *Biometrics*, 68(2):331–343.

Tan, J., Liang, D., Guan, Y., and Huang, H. (2024a). Graphical principal component analy-

sis of multivariate functional time series. *Journal of the American Statistical Association*, pages 1–24.

Tan, J., Shi, P., and Zhang, A. R. (2024b). Functional singular value decomposition. *arXiv preprint arXiv:2410.03619*.

Tan, J., Zhang, G., Wang, X., Huang, H., and Yao, F. (2024c). Green’s matching: an efficient approach to parameter estimation in complex dynamic systems. *Journal of the Royal Statistical Society Series B: Statistical Methodology*, 86(5):1266–1285.

Tian, M., Chen, B., Guo, A., Jiang, S., and Zhang, A. R. (2024). Reliable generation of privacy-preserving synthetic electronic health record time series via diffusion models. *Journal of the American Medical Informatics Association*, 31(11):2529–2539.

Tong, A., Fatras, K., Malkin, N., Huguet, G., Zhang, Y., Rector-Brooks, J., Wolf, G., and Bengio, Y. (2024). Improving and generalizing flow-based generative models with minibatch optimal transport. *Transactions on Machine Learning Research*, pages 1–34.

Van der Vaart, A. W. (2000). *Asymptotic statistics*, volume 3. Cambridge university press.

Vincent, P. (2011). A connection between score matching and denoising autoencoders. *Neural computation*, 23(7):1661–1674.

Wainwright, M. J. (2019). *High-dimensional statistics: A non-asymptotic viewpoint*, volume 48. Cambridge university press.

Wang, J.-L., Chiou, J.-M., and Müller, H.-G. (2016). Functional data analysis. *Annual Review of Statistics and its application*, 3:257–295.

Wilson, A. G. and Ghahramani, Z. (2010). Copula processes. *Advances in Neural Information Processing Systems*, 23.

Wood, S. and Wood, M. S. (2015). Package ‘mgcv’. *R package version*, 1(29):729.

Wood, S. N. (2006). Low-rank scale-invariant tensor product smooths for generalized additive mixed models. *Biometrics*, 62(4):1025–1036.

Wood, S. N. (2011). Fast stable restricted maximum likelihood and marginal likelihood estimation of semiparametric generalized linear models. *Journal of the Royal Statistical Society Series B: Statistical Methodology*, 73(1):3–36.

Wu, S., Yang, J., Xu, G., and Zhu, J. (2025). Denoising diffused embeddings: a generative approach for hypergraphs. *arXiv preprint arXiv:2501.01541*.

Yao, F. (2007). Functional principal component analysis for longitudinal and survival data. *Statistica Sinica*, 17:965–983.

Yao, F., Müller, H.-G., Clifford, A. J., Dueker, S. R., Follett, J., Lin, Y., Buchholz, B. A., and Vogel, J. S. (2003). Shrinkage estimation for functional principal component scores with application to the population kinetics of plasma folate. *Biometrics*, 59(3):676–685.

Yao, F., Müller, H.-G., and Wang, J.-L. (2005). Functional data analysis for sparse longitudinal data. *Journal of the American statistical association*, 100(470):577–590.

Yoon, J., Mizrahi, M., Ghalaty, N. F., Jarvinen, T., Ravi, A. S., Brune, P., Kong, F., Anderson, D., Lee, G., Meir, A., et al. (2023). Ehr-safe: generating high-fidelity and privacy-preserving synthetic electronic health records. *NPJ digital medicine*, 6(1):141.

Yuan, M. and Cai, T. T. (2010). A reproducing kernel hilbert space approach to functional linear regression. *The Annals of Statistics*, 38(6):3412–3444.

Zeidler, E. (1985). *Nonlinear functional analysis and its applications: I: Fixed-Point Theorems*. Springer Verlag.

Zhang, Z., Wang, X., Kong, L., and Zhu, H. (2022). High-dimensional spatial quantile function-on-scalar regression. *Journal of the American Statistical Association*, 117(539):1563–1578.

A Theoretical Proofs

A.1 Proof of Proposition 1

Proof. The marginal distributions of X and Z are denoted as F_t and $F_{t,\text{base}}$, respectively.

Define $g_t(x) = F_t^{-1} \circ F_{t,\text{base}}(x)$. Thus, g_t is a continuous and strictly increasing function between $\text{supp}(Z(t))$ and $\text{supp}(X(t))$.

If $X(\cdot)$ is a copula process with a base process $Z(\cdot)$, define

$$\tilde{Z}(t) = F_{t,\text{base}}^{-1}(F_t(X(t))).$$

For any $t_1, \dots, t_m \in \mathcal{T}$ and $x_1 \in \text{supp}(Z(t_1)), \dots, x_m \in \text{supp}(Z(t_m))$,

$$\begin{aligned} & \mathbb{P}\{\tilde{Z}(t_1) \leq x_1, \dots, \tilde{Z}(t_m) \leq x_m\} \\ &= \mathbb{P}\{F_{t_1}(X(t_1)) \leq F_{t_1,\text{base}}(x_1), \dots, F_{t_m}(X(t_m)) \leq F_{t_m,\text{base}}(x_m)\} \\ &= c_{t_1, \dots, t_m}(F_{t_1,\text{base}}(x_1), \dots, F_{t_m,\text{base}}(x_m)) \\ &= H_{\text{base}}(x_1, \dots, x_m; t_1, \dots, t_m) \\ &= \mathbb{P}\{Z(t_1) \leq x_1, \dots, Z(t_m) \leq x_m\}. \end{aligned}$$

Then the stochastic processes $Z(\cdot)$ and $\tilde{Z}(\cdot)$ are equal in distribution.

Notice that

$$\begin{aligned} g_t(\tilde{Z}(t)) &= F_t^{-1} \circ F_{t,\text{base}}(F_{t,\text{base}}^{-1}(F_t(X(t)))) \\ &= F_t^{-1} \circ F_t(X(t)) = X(t), \quad t \in \mathcal{T}. \end{aligned}$$

Thus, $X(t) = g_t(\tilde{Z}(t))$, almost surely, for all $t \in \mathcal{T}$. Therefore, $\{X(t)\}_{t \in \mathcal{T}}$ and $\{g_t(Z(t))\}_{t \in \mathcal{T}}$ are equal in distribution.

Conversely, we assume that there exists a process $\tilde{Z}(\cdot)$ with the same distribution as $Z(\cdot)$, and a continuous and strictly increasing function g_t on \mathbb{R} for each $t \in \mathcal{T}$, such that

$X(t) = g_t(\tilde{Z}(t))$, $t \in \mathcal{T}$. We first claim that

$$\tilde{Z}(t) = F_{t,\text{base}}^{-1}(F_t(X(t))), \text{ almost surely, } \forall t \in \mathcal{T}.$$

This can be proven, by noting that

$$\tilde{Z}(t) = g_t^{-1}(X(t)) \text{ and } F_{t,\text{base}}^{-1}(F_t(X(t)))$$

have the same distribution for each $t \in \mathcal{T}$. Since g_t^{-1} and $F_{t,\text{base}}^{-1} \circ F_t$ are both continuous and strictly increasing functions of $x \in \text{supp}(X(t))$, $\forall t \in \mathcal{T}$. Then by Lemma S1, $g_t^{-1}(X(t)) = F_{t,\text{base}}^{-1}(F_t(X(t)))$, almost surely. Claim holds.

Notice that For any $t_1, \dots, t_m \in \mathcal{T}$ and $u_1, \dots, u_m \in [0, 1]$,

$$\begin{aligned} & c_{t_1, \dots, t_m}(u_1, \dots, u_m) \\ &= \mathbb{P}(F_{t_1}(X(t_1)) \leq u_1, \dots, F_{t_m}(X(t_m)) \leq u_m) \\ &= \mathbb{P}(F_{t_1, \text{base}}^{-1} \circ F_{t_1}(X(t_1)) \leq F_{t_1, \text{base}}^{-1}(u_1), \dots, F_{t_m, \text{base}}^{-1} \circ F_{t_m}(X(t_m)) \leq F_{t_m, \text{base}}^{-1}(u_m)) \\ &= \mathbb{P}\{\tilde{Z}(t_1) \leq F_{t_1, \text{base}}^{-1}(u_1), \dots, \tilde{Z}(t_m) \leq F_{t_m, \text{base}}^{-1}(u_m)\} \\ &= \mathbb{P}\{Z(t_1) \leq F_{t_1, \text{base}}^{-1}(u_1), \dots, Z(t_m) \leq F_{t_m, \text{base}}^{-1}(u_m)\}. \end{aligned}$$

Then $X(\cdot)$ is a copula process upon a base process $Z(\cdot)$. We then complete the proof. □

A.2 Proof of Theorem 1

Proof. (a) is a direct result of Lemma S2. We just prove (b), (c), and (d) of Theorem 1 in the following.

(b) We first claim that $\phi_{1,t}(x)$ is strictly increasing in x . Therefore, $\phi_{1,t}(\cdot)$ is injective and thus a bijection onto its image. Suppose for contradiction that $x_1 < x_2$, but $\phi_{1,t}(x_1) \geq$

$\phi_{1,t}(x_2)$. Since $\phi_{u,t}(x)$ is continuous in u , and

$$\phi_{0,t}(x_1) = x_1 < x_2 = \phi_{0,t}(x_2),$$

the intermediate value theorem implies that there exists a first time $u_0 \in (0, 1]$ such that the trajectories meet:

$$\phi_{u_0,t}(x_1) = \phi_{u_0,t}(x_2).$$

By Lemma S2, we must have $x_1 = x_2$, which leads to a contradiction. Therefore, we have $\phi_{1,t}(x_1) < \phi_{1,t}(x_2)$. Claim holds.

Define $\psi_{u,t}(z) = \phi_{1-u,t}(\phi_{1,t}^{-1}(z))$. Notice that $\psi_{0,t}(z) = z$ and $\psi_{1,t}(z) = \phi_{1,t}^{-1}(z)$. Besides,

$$\frac{\partial \psi_{u,t}(z)}{\partial u} = \frac{\partial \phi_{1-u,t} \circ \phi_{1,t}^{-1}(z)}{\partial u} = -V_{1-u,t}(\phi_{1-u,t} \circ \phi_{1,t}^{-1}(z)) = -V_{1-u,t}(\psi_{u,t}(z)).$$

We then complete the proof.

(c) We first prove that $\phi_{u,t}(x)$ is a continuous function of x . To this end, we integrate from 0 to u :

$$\phi_{u,t}(x) = x + \int_0^u V_{s,t}(\phi_{s,t}(x)) \, ds.$$

Consider two points x_1 and x_2 , with solutions:

$$\begin{aligned} \phi_{u,t}(x_1) &= x_1 + \int_0^u V_{s,t}(\phi_{s,t}(x_1)) \, ds, \\ \phi_{u,t}(x_2) &= x_2 + \int_0^u V_{s,t}(\phi_{s,t}(x_2)) \, ds. \end{aligned}$$

Subtracting the equations and taking absolute values, the Lipschitz continuity of V implies that

$$\begin{aligned} |\phi_{u,t}(x_1) - \phi_{u,t}(x_2)| &\leq |x_1 - x_2| + \int_0^u |V_{s,t}(\phi_{s,t}(x_1)) - V_{s,t}(\phi_{s,t}(x_2))| \, ds \\ &\leq |x_1 - x_2| + L \int_0^u |\phi_{s,t}(x_1) - \phi_{s,t}(x_2)| \, ds. \end{aligned}$$

Let $\delta(s) = |\phi_{s,t}(x_1) - \phi_{s,t}(x_2)|$. Then

$$\delta(u) \leq |x_1 - x_2| + L \int_0^u \delta(s) \, ds.$$

Applying Grönwall's inequality, we have

$$\delta(u) \leq |x_1 - x_2| \cdot e^{Lu}. \quad (28)$$

Then $\phi_{u,t}(x)$ is a continuous function of x .

Notice that

$$\phi_{1,t}(Z(t)) \stackrel{d}{=} F_t^{-1} \circ F_{t,\text{base}}(Z(t)),$$

where $\phi_{1,t}$ and $F_t^{-1} \circ F_{t,\text{base}}$ are both strictly increasing and continuous functions. Then,

$$\phi_{1,t}(Z_0(t)) = F_t^{-1} \circ F_{t,\text{base}}(Z_0(t)), \text{ almost surely,}$$

by Lemma S1. Since $Z_0(t)$ is a continuous random variable,

$$\phi_{1,t}(z) = F_t^{-1} \circ F_{t,\text{base}}(z), \text{ almost surely,}$$

for Lebesgue-almost every $z \in \text{supp}(Z_0(t))$, according to Lemma S3.

Furthermore, notice that for each t ,

$$\mathbb{P}(\phi_{1,t}^{-1}(Z_1(t)) \leq z) = \mathbb{P}(Z_1(t) \leq \phi_{1,t}^{-1}(z)) = \mathbb{P}(\phi_{1,t}(Z_0(t)) \leq \phi_{1,t}(z)) = \mathbb{P}(Z_0(t) \leq z).$$

Then

$$\phi_{1,t}^{-1}(Z_1(t)) \stackrel{d}{=} F_{t,\text{base}}^{-1} \circ F_t(Z_1(t)), \quad t \in \mathcal{T}.$$

We similarly prove that for each $t \in \mathcal{T}$,

$$\phi_{1,t}^{-1}(x) = F_{t,\text{base}}^{-1} \circ F_t(x),$$

for Lebesgue-almost every $x \in \text{supp}(Z_1(t))$.

(d) For any $x_1 \in \text{supp}(X(t_1)), \dots, x_m \in \text{supp}(X(t_m))$,

$$\begin{aligned} & \mathbb{P}(X(t_1) \leq x_1, \dots, X(t_m) \leq x_m) \\ &= \mathbb{P}(F_{t_1}(X(t_1)) \leq F_{t_1}(x_1), \dots, F_{t_m}(X(t_m)) \leq F_{t_m}(x_m)) \\ &= H_{\text{base}}(F_{t_1,\text{base}}^{-1} \circ F_{t_1}(x_1), \dots, F_{t_m,\text{base}}^{-1} \circ F_{t_m}(x_m); t_1, \dots, t_m) \\ &= \mathbb{P}(Z_0(t_1) \leq F_{t_1,\text{base}}^{-1} \circ F_{t_1}(x_1), \dots, Z_0(t_m) \leq F_{t_m,\text{base}}^{-1} \circ F_{t_m}(x_m)). \end{aligned}$$

By (c), we have

$$\begin{aligned}
& \mathbb{P}(Z_0(t_1) \leq F_{t_1, \text{base}}^{-1} \circ F_{t_1}(x_1), \dots, Z_0(t_m) \leq F_{t_m, \text{base}}^{-1} \circ F_{t_m}(x_m)) \\
&= \mathbb{P}(\phi_{1,t_1}(Z_0(t_1)) \leq x_1, \dots, \phi_{1,t_m}(Z_0(t_m)) \leq x_m) \\
&= \mathbb{P}(Z_1(t_1) \leq x_1, \dots, Z_1(t_m) \leq x_m).
\end{aligned}$$

Therefore, X and Z_1 are equal in distribution. □

A.3 Proof of Theorem 2

Proof. Denote $V_{u,t}(x) = V(u, t, x)$. We claim that if $h \in W_2^q(\mathcal{T})$, then

$$\begin{aligned}
& \frac{d^q}{dt^q} V(u, t, h(t)) \\
&= \sum_{m=0}^q \sum_{\substack{l=0 \\ k_1+2k_2+\dots+(q-m)k_{q-m}=q-m \\ k_1+k_2+\dots+k_{q-m}=l}}^{q-m} C_{k_1, \dots, k_{q-m}, m, l} \frac{\partial^{l+m} V}{\partial t^m \partial x^l} \prod_{j=1}^{q-m} (h^{(j)}(t))^{k_j}, \quad (29)
\end{aligned}$$

where $C_{k_1, \dots, k_{q-m}, m, q}$ s are some constants. We first evaluate the formula for $q = 1$, which is

$$\begin{aligned}
\frac{d}{dt} V(u, t, h(t)) &= \frac{\partial V}{\partial t} + \frac{\partial V}{\partial x} h'(t) \\
&= C_{1,0,1} \frac{\partial V}{\partial x} h'(t) + C_{0,1,0} \frac{\partial V}{\partial t}.
\end{aligned}$$

where $C_{1,0,1} = C_{0,1,0} = 1$. We then assume (29) holds for $q = n$. For $q = n + 1$, we evaluate

$$\frac{d}{dt} \left(\frac{\partial^{l+m} V}{\partial t^m \partial x^l} \prod_{j=1}^{n-m} (h^{(j)}(t))^{k_j} \right)$$

Define: $A(t) = \frac{\partial^{l+m} V}{\partial t^m \partial x^l}(u, t, h(t))$ and $B(t) = \prod_{j=1}^{n-m} (h^{(j)}(t))^{k_j}$. Then, the derivative is:

$$\frac{d}{dt} [A(t)B(t)] = A'(t)B(t) + A(t)B'(t).$$

Note that

$$\begin{aligned}
A'(t) &= \frac{\partial^{l+m+1}V}{\partial t^{m+1}\partial x^l}(u, t, h(t)) + \frac{\partial^{l+m+1}V}{\partial t^m\partial x^{l+1}}(u, t, h(t)) \cdot h'(t) \\
B'(t) &= \sum_{p=1}^{n-m} \left[\frac{d}{dt} (h^{(p)}(t))^{k_p} \right] \prod_{j \neq p} (h^{(j)}(t))^{k_j} \\
&= \sum_{p=1}^{n-m} \left[k_p (h^{(p)}(t))^{k_p-1} h^{(p+1)}(t) \right] \prod_{j \neq p} (h^{(j)}(t))^{k_j}
\end{aligned}$$

Combining these, the derivative is:

$$\begin{aligned}
&\frac{d}{dt} \left(\frac{\partial^{l+m}V}{\partial t^m\partial x^l} \prod_{j=1}^{n-m} (h^{(j)}(t))^{k_j} \right) \\
&= \left(\frac{\partial^{l+m+1}V}{\partial t^{m+1}\partial x^l} + \frac{\partial^{l+m+1}V}{\partial t^m\partial x^{l+1}} h'(t) \right) \prod_{j=1}^{n-m} (h^{(j)}(t))^{k_j} \\
&\quad + \frac{\partial^{l+m}V}{\partial t^m\partial x^l} \sum_{p=1}^{n-m} k_p (h^{(p)}(t))^{k_p-1} h^{(p+1)}(t) \prod_{j \neq p} (h^{(j)}(t))^{k_j}.
\end{aligned}$$

Therefore,

$$\begin{aligned}
& \frac{d^{n+1}}{dt^{n+1}} V(u, t, h(t)) \\
&= \sum_{m=0}^n \sum_{l=0}^{n-m} \sum_{\substack{k_1+2k_2+\dots+(n-m)k_{n-m}=n-m \\ k_1+k_2+\dots+k_{n-m}=l}} C_{k_1, \dots, k_{n-m}, m, l} \frac{d}{dt} \left(\frac{\partial^{l+m} V}{\partial t^m \partial x^l} \prod_{j=1}^{n-m} (h^{(j)}(t))^{k_j} \right) \\
&= \sum_{m=0}^n \sum_{l=0}^{n-m} \sum_{\substack{k_1+2k_2+\dots+(n-m)k_{n-m}=n-m \\ k_1+k_2+\dots+k_{n-m}=l}} C_{k_1, \dots, k_{n-m}, m, l} \left\{ \left(\frac{\partial^{l+m+1} V}{\partial t^{m+1} \partial x^l} + \frac{\partial^{l+m+1} V}{\partial t^m \partial x^{l+1}} h'(t) \right) \right. \\
&\quad \left. \prod_{j=1}^{n-m} (h^{(j)}(t))^{k_j} + \frac{\partial^{l+m} V}{\partial t^m \partial x^l} \sum_{p=1}^{n-m} k_p (h^{(p)}(t))^{k_p-1} h^{(p+1)}(t) \prod_{j \neq p} (h^{(j)}(t))^{k_j} \right\} \\
&= \sum_{m=0}^n \sum_{l=0}^{n-m} \sum_{\substack{k_1+2k_2+\dots+(n-m)k_{n-m}=n-m \\ k_1+k_2+\dots+k_{n-m}=l}} C_{k_1, \dots, k_{n-m}, m, l} \frac{\partial^{l+m+1} V}{\partial t^{m+1} \partial x^l} \prod_{j=1}^{n-m} (h^{(j)}(t))^{k_j} \\
&\quad + \sum_{m=0}^n \sum_{l=0}^{n-m} \sum_{\substack{k_1+2k_2+\dots+(n-m)k_{n-m}=n-m \\ k_1+k_2+\dots+k_{n-m}=l}} C_{k_1, \dots, k_{n-m}, m, l} \frac{\partial^{l+m+1} V}{\partial t^m \partial x^{l+1}} h'(t) \prod_{j=1}^{n-m} (h^{(j)}(t))^{k_j} \\
&\quad + \sum_{m=0}^n \sum_{l=0}^{n-m} \sum_{\substack{k_1+2k_2+\dots+(n-m)k_{n-m}=n-m \\ k_1+k_2+\dots+k_{n-m}=l}} C_{k_1, \dots, k_{n-m}, m, l} \\
&\quad \cdot \frac{\partial^{l+m} V}{\partial t^m \partial x^l} \sum_{p=1}^{n-m} k_p (h^{(p)}(t))^{k_p-1} h^{(p+1)}(t) \prod_{j \neq p} (h^{(j)}(t))^{k_j} \\
&= \sum_{m=1}^{n+1} \sum_{l=0}^{(n+1)-m} \sum_{\substack{k_1+2k_2+\dots+(n+1-m)k_{(n+1)-m}=(n+1)-m \\ k_1+k_2+\dots+k_{(n+1)-m}=l}} C_{k_1, \dots, k_{(n+1)-m}, m-1, l} \frac{\partial^{l+m} V}{\partial t^m \partial x^l} \cdot \prod_{j=1}^{(n+1)-m} (h^{(j)}(t))^{k_j} \\
&\quad + \sum_{m=0}^n \sum_{l=1}^{(n+1)-m} \sum_{\substack{(k_1+1)+2k_2+\dots+(n-m)k_{n-m}+(n+1-m)\cdot 0=(n+1)-m \\ (1+k_1)+k_2+\dots+k_{n-m}+0=l}} C_{k_1, \dots, k_{n-m}, m, l-1} \frac{\partial^{l+m} V}{\partial t^m \partial x^l} \\
&\quad \cdot (h'(t) \prod_{j=1}^{n-m} (h^{(j)}(t))^{k_j}) \\
&\quad + \sum_{m=0}^n \sum_{l=0}^{n-m} \sum_{p=1}^{n-m} \sum_{\substack{k_1+2k_2+\dots+p(k_p-1)+(p+1)(k_{p+1}+1)+\dots+(n-m)k_{n-m}+(n+1-m)\cdot 0=(n+1)-m \\ k_1+k_2+\dots+(k_p-1)+(k_{p+1}+1)+\dots+k_{n-m}+0=l}} k_p C_{k_1, \dots, k_{n-m}, m, l} \\
&\quad \cdot \frac{\partial^{l+m} V}{\partial t^m \partial x^l} \cdot \left((h^{(p)}(t))^{k_p-1} \cdot h^{(p+1)}(t) \cdot \prod_{j \neq p} (h^{(j)}(t))^{k_j} \right).
\end{aligned}$$

Therefore, $\frac{d^{n+1}}{dt^{n+1}}V(u, t, h(t))$ can be represented by

$$\sum_{m=0}^{n+1} \sum_{l=0}^{n+1-m} \sum_{\substack{k_1+2k_2+\dots+(n+1-m)k_{n+1-m}=n+1-m \\ k_1+k_2+\dots+k_{n+1-m}=l}} \tilde{C}_{k_1, \dots, k_{n+1-m}, m, l} \frac{\partial^{l+m} V}{\partial t^m \partial x^l} \prod_{j=1}^{n+1-m} (h^{(j)}(t))^{k_j},$$

where $\tilde{C}_{k_1, \dots, k_{q-m}, m, q}$ s are some constants determined by $C_{k_1, \dots, k_{q-m}, m, q}$ s. Claim holds.

Note that $\frac{\partial^{l+m} V}{\partial t^m \partial x^l} \in L^2(\mathcal{T})$, $h^{(q)} \in L^2(\mathcal{T})$, k_q in (29) is always 0 or 1, and $h^{(j)}$ is a continuous function for $j < q$, then $\frac{d^q}{dt^q}V(u, t, h(t))$ is a function of t contained in $L^2(\mathcal{T})$. Therefore, $V_{u, \cdot}(h(\cdot)) \in W_q^2(\mathcal{T})$ whenever $h(\cdot) \in W_q^2(\mathcal{T})$.

Under conditions (10) and (11), and assuming $Z_0 \in W_q^2(\mathcal{T})$, the solution Z_u to (9) lies in $W_q^2(\mathcal{T})$ by Lemma S2.

□

The following proposition is a direct result of Theorem 2.

Proposition S1 (Runge-Kutta Method for Smooth Function Generation). Let $\{u_1, \dots, u_M\}$ be an equally spaced sequence of $[0, 1]$ with a sufficiently small gap Δu . Given $Z_0(t)$ and $V_{u, t}$, define

$$Z_{u_{m+1}}(t) = Z_{u_m}(t) + \frac{\Delta u}{6} \{k_{1,m}(t) + 2k_{2,m}(t) + 2k_{3,m}(t) + k_{4,m}(t)\}, \quad t \in \mathcal{T}, \quad (30)$$

where $k_{1,m}(t) = V_{u_m, t}(Z_{u_m}(t))$, $k_{2,m}(t) = V_{u_m + \Delta u/2, t}(Z_{u_m}(t) + \Delta u \cdot k_{1,m}(t)/2)$, $k_{3,m}(t) = V_{u_m + \Delta u/2, t}(Z_{u_m}(t) + \Delta u \cdot k_{2,m}(t)/2)$, and $k_{4,m}(t) = V_{u_m + \Delta u, t}(Z_{u_m}(t) + \Delta u \cdot k_{3,m}(t))$. Suppose that $Z_0 \in W_q^2(\mathcal{T})$ and the vector field $V_{u, t}$ satisfies (10). Then

$$Z_{u_m} \in W_q^2(\mathcal{T}), \quad m = 1, \dots, M.$$

A.4 Proof of Theorem 3

Proof. We first show that $Z_u(t)$, generated by the vector field $V_{u,t}$ with initial condition $Z_0(t) \sim p_{0,t}$, has the probability density $p_{u,t}$. Our task is to prove that $p_{u,t}(x)$ satisfies continuity equation associated with the vector field $V_{u,t}$, i.e.,

$$\frac{\partial p_{u,t}(x)}{\partial u} = -\frac{\partial}{\partial x} (p_{u,t}(x) V_{u,t}(x)).$$

Therefore, $p_{u,t}$ is the density of $Z_u(t)$ for each t .

Notice that

$$\frac{\partial p_{u,t}(x)}{\partial u} = \int \frac{\partial}{\partial u} p_{u,t}(x | y) f_X(y; t) dy.$$

Since $V_{u,t}(\cdot | y)$ generates $p_{u,t}(\cdot | y)$, $p_{u,t}(\cdot | y)$ satisfies the continuity equation associated with the vector field $V_{u,t}(\cdot | y)$:

$$\frac{\partial p_{u,t}(x | y)}{\partial u} = -\frac{\partial}{\partial x} (p_{u,t}(x | y) V_{u,t}(x | y)).$$

Thus,

$$\begin{aligned} \frac{\partial p_{u,t}(x)}{\partial u} &= \int \left[-\frac{\partial}{\partial x} (p_{u,t}(x | y) V_{u,t}(x | y)) \right] f_X(y; t) dy \\ &= -\frac{\partial}{\partial x} \int p_{u,t}(x | y) V_{u,t}(x | y) f_X(y; t) dy. \end{aligned} \tag{31}$$

Meanwhile, notice that

$$V_{u,t}(x) = \int_{\text{supp}(p_{u,t})} V_{u,t}(x | z) \cdot \frac{p_{u,t}(x | z) f_X(z; t)}{p_{u,t}(x)} dz,$$

then $p_{u,t}(x) V_{u,t}(x) = \int_{\text{supp}(p_{u,t})} V_{u,t}(x | z) p_{u,t}(x | z) f_X(z; t) dz$. Since $p_{u,t}(x | z) f_X(z; t) \geq 0$ and $\int p_{u,t}(x | z) f_X(z; t) dz = 0$ for $x \notin \text{supp}(p_{u,t})$, we have $p_{u,t}(x | z) f_X(z; t) = 0$ for $x \notin \text{supp}(p_{u,t})$. It follows that

$$p_{u,t}(x) V_{u,t}(x) = \int V_{u,t}(x | z) p_{u,t}(x | z) f_X(z; t) dz,$$

and therefore,

$$-\frac{\partial}{\partial x} (p_{u,t}(x)V_{u,t}(x)) = -\frac{\partial}{\partial x} \int V_{u,t}(x \mid z)p_{u,t}(x \mid z)f_X(z; t) \, dz.$$

Combining the above inequality with (31), we have:

$$\frac{\partial p_{u,t}(x)}{\partial u} = -\frac{\partial}{\partial x} (p_{u,t}(x)V_{u,t}(x)).$$

Since the vector field $V_{u,t}$ is Lipschitz, the solution of Z_u is unique. Thus,

$$Z_u(t) \sim p_{u,t},$$

$t \in \mathcal{T}$ and $u \in [0, 1]$. In other word, the distributions of $Z_u(t)$ in (12) and (16) are the same. In the following proof, we do not distinguish between $Z_u(t)$ in (12) and (16).

Recall the objective of flow matching is to solve

$$\min_U \mathbb{E} \left\{ \frac{\partial Z_u(T)}{\partial u} - U(u, t, Z_u(T)) \right\}^2 \, du.$$

For $T = t$,

$$\begin{aligned}
& \mathbb{E} \left\{ \frac{\partial Z_u(t)}{\partial u} - U(u, t, Z_u(t)) \right\}^2 \\
&= \mathbb{E} \{V_{u,t}(Z_u(t)) - U(u, t, Z_u(t))\}^2 \\
&= \mathbb{E} [\mathbb{E} \{V_{u,t}(Z_u(t)) - U(u, t, Z_u(t))\}^2 \mid X(t)] \\
&= \mathbb{E} \left[\mathbb{E} \left\{ \int_{\text{supp}(p_{u,t})} V_{u,t}(Z_u(t) \mid x) \cdot \frac{p_{u,t}(Z_u(t) \mid x) \cdot f_X(x; t)}{p_{u,t}(Z_u(t))} dx - U(u, t, Z_u(t)) \right\}^2 \mid X(t) \right] \\
&= \mathbb{E} \left[\mathbb{E} \left\{ \int_{\text{supp}(p_{u,t})} V_{u,t}(Z_u(t) \mid x) \cdot \frac{p_{u,t}(Z_u(t) \mid x) \cdot f_X(x; t)}{p_{u,t}(Z_u(t))} dx \right\}^2 \mid X(t) \right] \\
&\quad - 2 \mathbb{E} \left[\mathbb{E} \int_{\text{supp}(p_{u,t})} V_{u,t}(Z_u(t) \mid x) \cdot \frac{p_{u,t}(Z_u(t) \mid x) \cdot f_X(x; t)}{p_{u,t}(Z_u(t))} dx \cdot U(u, t, Z_u(t)) \mid X(t) \right] \\
&\quad + \mathbb{E} \{ \mathbb{E} [U^2(u, t, Z_u(t)) \mid X(t)] \} \\
&= C - 2 \int_{\text{supp}(p_{u,t})} \int_{\text{supp}(p_{u,t})} \int_{\mathbb{R}} V_{u,t}(y \mid x) \cdot \frac{p_{u,t}(y \mid x) \cdot f_X(x; t)}{p_{u,t}(y)} \cdot U(u, t, y) \\
&\quad \cdot p_{u,t}(y \mid z) f_X(z; t) dx dy dz \\
&\quad + \mathbb{E} \{ \mathbb{E} [U^2(u, t, Z_u(t)) \mid X(t)] \} \\
&= C - 2 \int_{\mathbb{R}} \int_{\text{supp}(p_{u,t})} V_{u,t}(y \mid x) \cdot p_{u,t}(y \mid x) \cdot f_X(x; t) \cdot U(u, t, y) dx dy \\
&\quad + \mathbb{E} \{ \mathbb{E} [U^2(u, t, Z_u(t)) \mid X(t)] \} \\
&= C - 2 \mathbb{E} \{ \mathbb{E} [V_{u,t}(Z_u(t) \mid X(t)) \cdot U(u, t, Z_u(t)) \mid X(t)] \} + \mathbb{E} \{ \mathbb{E} [U^2(u, t, Z_u(t)) \mid X(t)] \} \\
&= \mathbb{E} [\mathbb{E} \{V_{u,t}(Z_u(t) \mid X(t)) - U(u, t, Z_u(t))\}^2 \mid X(t)] + C \\
&= \mathbb{E} \left\{ \mathbb{E} \left(\frac{\partial Z_u(t)}{\partial u} - U(u, t, Z_u(t)) \right)^2 \mid X(t) \right\} + C,
\end{aligned}$$

where C can take different values, containing terms that are independent of U . Let the

density of T be p_T . Then

$$\begin{aligned}
& \int_0^1 \mathbb{E} \left\{ \frac{\partial Z_u(T)}{\partial u} - U(u, t, Z_u(T)) \right\}^2 du \\
&= \int_0^1 \int_{\mathcal{T}} \mathbb{E} \left\{ \frac{\partial Z_u(t)}{\partial u} - U(u, t, Z_u(t)) \right\}^2 p_T(t) dt du \\
&= \int_0^1 \int_{\mathcal{T}} \mathbb{E} \left\{ \mathbb{E} \left(\frac{\partial Z_u(t)}{\partial u} - U(u, t, Z_u(t)) \right)^2 \mid X(t) \right\} p_T(t) dt du + C \\
&= \int_0^1 \mathbb{E} \left\{ \mathbb{E} \left(\frac{\partial Z_u(T)}{\partial u} - U(u, t, Z_u(T)) \right)^2 \mid X, T \right\} du + C.
\end{aligned}$$

The proof is complete. \square

A.5 Proof of Theorem S1

Theorem S1 (Reverse Representation of Rectified Flow Matching). Let V be a minimizer of (18). Define the inverse rectified flow matching:

$$\min_U \int_0^1 \mathbb{E} \left\{ Z_0(T) - X(T) - U(u, t, Z_u^{\text{inv}}(T)) \right\}^2 du, \quad (32)$$

where $Z_0(t) \sim p_{0,t}$, $X(t) \sim f_X(\cdot; t)$, $t \in \mathcal{T}$, and $Z_u^{\text{inv}}(t) = (1-u)X(t) + uZ_0(t)$, $u \in [0, 1]$; Z_0 , X , and T , are independent. Define

$$V_{\text{inv}}(u, t, x) = -V(1-u, t, x), \quad (33)$$

for all $u \in [0, 1]$, $t \in \mathcal{T}$, and $x \in \text{supp}(Z_u^{\text{inv}}(t))$. Then V_{inv} is a minimal vector field of (32).

Proof. The vector field V is obtained from the optimization problem:

$$V := \arg \min_U \int_0^1 \mathbb{E} \left[(X(T) - Z_0(T) - U(u, T, Z_u(T)))^2 \right] du$$

where $Z_u(t) = (1-u)Z_0(t) + uX(t)$, $Z_0(t) \sim p_{0,t}$, $X(t) \sim f_X(\cdot; t)$. The inverse problem is:

$$V_{\text{inv}} := \arg \min_U \int_0^1 \mathbb{E} \left[(Z_0(T) - X(T) - U(u, T, Z_u^{\text{inv}}(T)))^2 \right] du,$$

where $Z_u^{\text{inv}}(t) = (1 - u)X(t) + uZ_0(t)$. Note that

$$Z_{1-u}(t) = (1 - (1 - u))Z_0(t) + (1 - u)X(t) = uZ_0(t) + (1 - u)X(t) = Z_u^{\text{inv}}(t).$$

Then

$$\begin{aligned} V_{\text{inv}} &= \arg \min_U \int_{\mathcal{T}} \int_0^1 \mathbb{E} [(Z_0(t) - X(t) - U(u, t, Z_{1-u}(t)))^2] p_T(t) du dt, \\ &= \arg \min_U \int_{\mathcal{T}} \int_0^1 \mathbb{E} [(X(t) - Z_0(t) + U(1 - u, t, Z_u(t)))^2] p_T(t) du dt \\ &= \arg \min_U \int_{\mathcal{T}} \int_0^1 \mathbb{E} [X(t) - Z_0(t) - (-U(1 - u, t, Z_u(t)))]^2 p_T(t) du dt \\ &= \arg \min_U \int_{\mathcal{T}} \int_0^1 \mathbb{E} [X(t) - Z_0(t) - W(u, t, Z_u(t))]^2 p_T(t) du dt, \end{aligned}$$

where $W(u, t, x) = -U(1 - u, t, x)$. It follows that

$$-V_{\text{inv}}(1 - u, t, x) = V(u, t, x).$$

for all $u \in [0, 1]$, $t \in \mathcal{T}$, and $x \in \text{supp}(Z_u^{\text{inv}}(t))$. We complete the proof. \square

A.6 Proof of Theorem 4

For two sequences of non-negative real values $\{a_n\}$ and $\{b_n\}$, we say $a_n \lesssim b_n$ or $b_n \gtrsim a_n$ if there exists a constant $C > 0$ such that $a_n \leq Cb_n$ for all n .

Proof. We separate the proof into several parts.

Consistency of the vector field V . Let $\Omega = [0, 1] \times \mathcal{T} \times \mathcal{X}$, and denote the norm $\|\cdot\|$ as the $L^2(\Omega)$ norm, i.e., $\|\cdot\| \equiv \|\cdot\|_{L^2(\Omega)}$. We proceed to prove the theorem under the simplifying assumption that $\lambda_u = \lambda_t = \lambda_x = \lambda$. The proof for the more general case, where λ_u , λ_t , and λ_x differ, follows similarly.

Define $\|U\|_\infty = \sup_{u \in [0,1], t \in \mathcal{T}, x \in \mathcal{X}} |U(u, t, x)|$. Write $\mathbb{B}_{L_V} = \mathbb{B}_{L_V, 4}([0, 1], \mathcal{T}, \mathcal{X})$. Recall that $\hat{V} \in \mathbb{B}_{L_V}$ minimizes

$$\begin{aligned} & \mathcal{L}_n(U) + \mathcal{J}(U) \\ &= \frac{1}{n} \sum_{i=1}^n \frac{1}{J_i} \sum_{j=1}^{J_i} \int_0^1 \mathbb{E} \left[\left\{ X_i(T_{ij}) - Z_0(T_{ij}) - U(u, T_{ij}, Z_{u,i}(T_{ij})) \right\}^2 \mid X_i, T_{ij} \right] du \\ & \quad + \lambda \mathcal{J}(U), \end{aligned}$$

where $\mathcal{J}(U) = \int_{\mathcal{X}} \int_{\mathcal{T}} \int_0^1 \left\{ \left(\frac{\partial^2 U}{\partial u^2} \right)^2 + \left(\frac{\partial^2 U}{\partial t^2} \right)^2 + \left(\frac{\partial^2 U}{\partial x^2} \right)^2 \right\} du dt dx$. Let $\mathcal{L}(U) = E\{\mathcal{L}_n(U)\}$ denote the population loss, then $V = \arg \min_U \mathcal{L}(U)$.

Define $V^* = \arg \min_{U \in B_{L_V}} \mathcal{L}(U)$. As $V \in \mathcal{W}_2^2(\Omega)$, V^* can approximate V in the sense that (de Boor and DeVore, 1983)

$$\|V^* - V\|^2 = o(1),$$

as $L_V \rightarrow \infty$. Similarly, we have $\mathcal{J}(V^*) = O(1)$ and $\|V^*\| = O(1)$ as $L_V \rightarrow \infty$, since $\mathcal{J}(V)$ is bounded and $\|V\| = O(1)$ (Assumption 4). Notice that V^* is the minimizer of \mathcal{L} on the closed convex set B_{L_V} . By the Hilbert projection theorem (Theorem 2.5.1 in Hsing and Eubank (2015)), we have

$$\begin{aligned} & \mathcal{L}(U) - \mathcal{L}(V^*) \\ &= \int_0^1 \mathbb{E}_{T, Z_u} \left\{ V(u, T, Z_u(T)) - U(u, T, Z_u(T)) \right\}^2 du \\ & \quad - \int_0^1 \mathbb{E}_{T, Z_u} \left\{ V(u, T, Z_u(T)) - V^*(u, T, Z_u(T)) \right\}^2 du \\ &\geq \int_0^1 \mathbb{E}_{T, Z_u} \left\{ U(u, T, Z_u(T)) - V^*(u, T, Z_u(T)) \right\}^2 du, \end{aligned}$$

for any $U \in B_{L_V}$, where $T \sim p_T$ and $Z_u(t) \sim p_{Z_u(t)}$, with T and Z_u being independent.

By the optimality of \hat{V} ,

$$\mathcal{L}_n(\hat{V}) + \lambda \mathcal{J}(\hat{V}) \leq \mathcal{L}_n(V^*) + \lambda \mathcal{J}(V^*).$$

Therefore,

$$\begin{aligned}
& \mathcal{L}(\hat{V}) - \mathcal{L}(V^*) \\
& \leq \mathcal{L}(\hat{V}) - \mathcal{L}(V^*) - \mathcal{L}_n(\hat{V}) - \lambda \mathcal{J}(\hat{V}) + \mathcal{L}_n(V^*) + \lambda \mathcal{J}(V^*) \\
& \leq \mathcal{L}_n(V^*) - \mathcal{L}(V^*) + \mathcal{L}(\hat{V}) - \mathcal{L}_n(\hat{V}) + \lambda \{\mathcal{J}(V^*) - \mathcal{J}(\hat{V})\} \\
& \lesssim \mathcal{L}_n(V^*) - \mathcal{L}(V^*) + \mathcal{L}(\hat{V}) - \mathcal{L}_n(\hat{V}) + \lambda,
\end{aligned}$$

where the final inequality is due to $\mathcal{J}(V^*) = O(1)$ and $\mathcal{J}(\hat{V}) \geq 0$. It follows that

$$\begin{aligned}
& \int_0^1 \mathbb{E}_{T, Z_u} \left\{ \hat{V}(u, T, Z_u(T)) - V(u, T, Z_u(T)) \right\}^2 du \\
& \lesssim \int_0^1 \mathbb{E}_{T, Z_u} \left\{ \hat{V}(u, T, Z_u(T)) - V^*(u, T, Z_u(T)) \right\}^2 du \\
& \quad + \int_0^1 \mathbb{E} \left\{ V^*(u, T, Z_u(T)) - V(u, T, Z_u(T)) \right\}^2 du \\
& \leq \mathcal{L}(\hat{V}) - \mathcal{L}(V^*) + \int_0^1 \mathbb{E} \left\{ V^*(u, T, Z_u(T)) - V(u, T, Z_u(T)) \right\}^2 du \\
& \lesssim \mathcal{L}_n(V^*) - \mathcal{L}(V^*) + \mathcal{L}(\hat{V}) - \mathcal{L}_n(\hat{V}) + \lambda \\
& \quad + \int_0^1 \mathbb{E} \left\{ V^*(u, T, Z_u(T)) - V(u, T, Z_u(T)) \right\}^2 du.
\end{aligned}$$

Notice that the densities p_T and $Z_u(t)$ are bounded,

$$\int_0^1 \mathbb{E} \left[\left\{ V^*(u, T_{ij}, Z_u(T_{ij})) - V(u, T_{ij}, Z_u(T_{ij})) \right\}^2 du \right] \lesssim \|V^* - V\|^2,$$

which means

$$\begin{aligned}
& \int_0^1 \mathbb{E}_{T_{ij}, Z_{u,i}} \left[\left\{ \hat{V}(u, T_{ij}, Z_{u,i}(T_{ij})) - V(u, T_{ij}, Z_{u,i}(T_{ij})) \right\}^2 du \right] \\
& \lesssim |\mathcal{L}_n(V^*) - \mathcal{L}(V^*)| + |\mathcal{L}(\hat{V}) - \mathcal{L}_n(\hat{V})| + \lambda + \|V^* - V\|^2.
\end{aligned}$$

As $\lambda + \|V^* - V\| = o(1)$, it remains to prove that

$$|\mathcal{L}_n(V^*) - \mathcal{L}(V^*)| + |\mathcal{L}(\hat{V}) - \mathcal{L}_n(\hat{V})| = o_p(1),$$

which implies

$$\int_0^1 \mathbb{E}_{T, Z_u} \left\{ \hat{V}(u, T, Z_u(T)) - V(u, T, Z_u(T)) \right\}^2 du = o_p(1). \quad (34)$$

Define

$$h_n(U) = \frac{1}{n} \sum_{i=1}^n \left[X_i(T_i) - \tilde{Z}_{0,i}(T_i) - U(W_i, T_i, \tilde{Z}_{W_i,i}(T_i)) \right]^2 - \mathcal{L}(U),$$

where $W_i \sim \text{Unif}([0, 1])$, $T_i \sim p_T$, and $\tilde{Z}_{0,i}(t) \sim p_{Z_0(t)}$, independently; $\tilde{Z}_{0,i} = (1-u)\tilde{Z}_{i,0}(t) + uX_i(t)$. The triplet $(W_i, T_i, \tilde{Z}_{0,i})$ are defined to match the i th function X_i , which are independent across i . Notice that

$$\begin{aligned} & \text{Var}(\mathcal{L}_n(U) - \mathcal{L}(U)) \\ &= \frac{1}{n^2} \sum_{i=1}^n \text{Var} \left(\frac{1}{J_i} \sum_{j=1}^{J_i} \int_0^1 \mathbb{E} \left[\left\{ X_i(T_{ij}) - Z_0(T_{ij}) - U(u, T_{ij}, Z_{u,i}(T_{ij})) \right\}^2 \mid X_i, T_{ij} \right] du \right) \\ &= \frac{1}{n^2} \sum_{i=1}^n \text{Var} \left(\mathbb{E} \frac{1}{J_i} \sum_{j=1}^{J_i} \left[\left\{ X_i(T_{ij}) - Z_0(T_{ij}) - U(W_i, T_{ij}, Z_{W_i,i}(T_{ij})) \right\}^2 \mid X_i, T_{ij} \right] \right) \\ &= \frac{1}{n^2} \sum_{i=1}^n \text{Var} \left(\mathbb{E} \frac{1}{J_i} \sum_{j=1}^{J_i} \left[\left\{ X_i(T_{ij}) - \tilde{Z}_{0,i}(T_{ij}) - U(W_i, T_{ij}, \tilde{Z}_{W_i,i}(T_{ij})) \right\}^2 \mid X_i, T_{ij} \right] \right) \\ &\leq \frac{1}{n^2} \sum_{i=1}^n \text{Var} \left(\frac{1}{J_i} \sum_{j=1}^{J_i} \left\{ X_i(T_{ij}) - \tilde{Z}_{0,i}(T_{ij}) - U(W_i, T_{ij}, \tilde{Z}_{W_i,i}(T_{ij})) \right\}^2 \right) \\ &\leq \frac{1}{n^2} \sum_{i=1}^n \text{Var} \left(\left\{ X_i(T_{ij}) - \tilde{Z}_{0,i}(T_{ij}) - U(W_i, T_{ij}, \tilde{Z}_{W_i,i}(T_{ij})) \right\}^2 \right) \\ &= \mathbb{E}(h_n(U))^2. \end{aligned} \quad (35)$$

Since $\mathbb{E}\|X_i\|^4$, $\mathbb{E}\|\tilde{Z}_{0,i}\|^4$, and $\|U\|_\infty$ are bounded, for $i = 1, \dots, n$ and $U \in \mathbb{B}_{L_V}$. Then $\sup_{n \geq 1} \mathbb{E} \sup_{U \in \mathbb{B}_{L_V}} h_n^4(U) < \infty$, which indicates that $\{\sup_{U \in \mathbb{B}_{L_V}} h_n^2(U); n \geq 1\}$ is uniformly integrable. As such, Theorem 2.20 in [Van der Vaart \(2000\)](#) indicates that

$$\sup_{U \in \mathbb{B}_{L_V}} |h_n(U)| = o_p(1) \quad (36)$$

implies $\mathbb{E} \sup_{U \in \mathbb{B}_{L_V}} (h_n(U))^2 = o(1)$, which further leads to

$$|\mathcal{L}(\hat{V}) - \mathcal{L}_n(\hat{V})| = o_p(1) \quad \text{and} \quad |\mathcal{L}_n(V^*) - \mathcal{L}(V^*)| = o_p(1),$$

due to (35). Then (34) holds.

It remains to establish (36). Note that the dimension of the functional space \mathbb{B}_{L_V} is L_V^3 , and therefore its Vapnik–Chervonenkis (VC) dimension is at most L_V^3 (see Proposition 4.20 in [Wainwright \(2019\)](#)). By the Glivenko–Cantelli theorem for empirical processes (see Theorems 2.4.3 and 2.6.7 in [?](#)), (36) holds if $\frac{L_V^3}{n} \rightarrow 0$. This follows directly from the assumption $L_V = o(n^{1/3})$, which completes the proof.

Consistency of the latent correlation function.

We prove that the estimator $\hat{\rho}$ is consistent to the true function ρ , i.e.,

$$\|\hat{\rho} - \rho\| = o_p(1), \quad \text{as } n \rightarrow \infty,$$

where the true function is defined as:

$$\rho(t, s) = E[\psi_{1,t}(X(t))\psi_{1,s}(X(s))], \quad t, s \in \mathcal{T},$$

and

$$\hat{\rho} = \arg \min_{f \in \mathbb{B}_{L_\rho, 4}(\mathcal{T}, \mathcal{T})} \frac{1}{n} \sum_{i=1}^n \frac{1}{J_i^2} \sum_{j_1, j_2=1}^{J_i} [G_i(T_{ij_1}, T_{ij_2}) - f(T_{ij_1}, T_{ij_2})]^2 + \lambda \mathcal{J}(f),$$

where $G_i(T_{ij_1}, T_{ij_2}) = \hat{\psi}_{1,T_{ij_1}}(X_i(T_{ij_1})) \cdot \hat{\psi}_{1,T_{ij_2}}(X_i(T_{ij_2}))$. Define:

$$\tilde{\rho}(t, s) = E_{X_i}[G_i(t, s)] = E_{X_i}[\hat{\psi}_{1,t}(X_i(t))\hat{\psi}_{1,s}(X_i(s))].$$

By the triangle inequality:

$$\|\hat{\rho} - \rho\| \leq \|\hat{\rho} - \tilde{\rho}\| + \|\tilde{\rho} - \rho\|.$$

In the following, we respectively show that $\|\hat{\rho} - \tilde{\rho}\| = o_p(1)$ and $\|\tilde{\rho} - \rho\| = o_p(1)$, which leads to

$$\|\hat{\rho} - \rho\| = o_p(1). \quad (37)$$

- Let $\delta_t(z) = \hat{\psi}_{1,t}(z) - \psi_{1,t}(z)$. Then:

$$\begin{aligned}
& \hat{\psi}_{1,t}(X_i(t))\hat{\psi}_{1,s}(X_i(s)) \\
&= \psi_{1,t}(X_i(t))\psi_{1,s}(X_i(s)) + \psi_{1,t}(X_i(t))\delta_s(X_i(s)) \\
&\quad + \psi_{1,s}(X_i(s))\delta_t(X_i(t)) + \delta_t(X_i(t))\delta_s(X_i(s)).
\end{aligned}$$

Taking expectations:

$$\begin{aligned}
\tilde{\rho}(t, s) &= \rho(t, s) + E_{X_i}[\psi_{1,t}(X_i(t))\delta_s(X_i(s))] + E_{X_i}[\psi_{1,s}(X_i(s))\delta_t(X_i(t))] \\
&\quad + E_{X_i}[\delta_t(X_i(t))\delta_s(X_i(s))] \\
&:= \rho(t, s) + A(t, s) + B(t, s) + C(t, s).
\end{aligned} \tag{38}$$

Notice that

$$\|A\| \leq \sqrt{\int_0^1 \mathbb{E}_{X_i} \psi_{1,t}^2(X_i(t)) dt} \cdot \sqrt{\mathbb{E}_{X_i} \int_0^1 \delta_t^2(X_i(t)) dt}. \tag{39}$$

We bound these two terms in the following.

- By the Alekseev–Gröbner formula,

$$\begin{aligned}
& \hat{\psi}_{1,t}(z) - \psi_{1,t}(z) \\
&= \int_0^1 \frac{d\hat{\psi}_{(u,1),t}(x)}{dx} \Big|_{x=\psi_{u,t}(z)} \cdot \left(V(1-u, t, \psi_{u,t}(z)) - \hat{V}(1-u, t, \psi_{u,t}(z)) \right) du,
\end{aligned}$$

where $\psi_{(u,v),t}(z)$ denotes the solution of (22) starting at u and ending at v , with initial value z . Then,

$$\begin{aligned}
& \mathbb{E}_{X_i} \int_0^1 \delta_t^2(X_i(t)) dt \\
&\leq \mathbb{E} \int_0^1 \int_0^1 \left(\frac{d\hat{\psi}_{(u,1),t}(z)}{dz} \Big|_{z=\psi_{u,t}(X_i(t))} \right)^2 \\
&\quad \cdot \left(\hat{V}(1-u, t, \psi_{u,t}(X_i(t))) - V(1-u, t, \psi_{u,t}(X_i(t))) \right)^2 du dt. \tag{40}
\end{aligned}$$

Notice that $\hat{\psi}_{(u,w),t}(z) = z - \int_u^w \hat{V}(1-v, t, \hat{\psi}_{(u,v),t}(z)) dv$,

$$\frac{d\hat{\psi}_{(u,w),t}(z)}{dz} = 1 - \int_u^w \frac{d\hat{V}(1-v, t, x)}{dx} \Big|_{x=\hat{\psi}_{(u,v),t}(z)} \cdot \frac{d\hat{\psi}_{(u,v),t}(z)}{dz} dv.$$

Denote the Lipschitz constant of $\hat{V}(\cdot, \cdot, x)$ with respect to x as L_1 . Therefore,

$$\frac{d}{dw} \left| \frac{d\hat{\psi}_{(u,w),t}(z)}{dz} \right| \leq L_1 \left| \frac{d\hat{\psi}_{(u,w),t}(z)}{dz} \right|.$$

Note that $\hat{\psi}_{(u,u),t}(z) = z$ and $\frac{d\hat{\psi}_{(u,u),t}(z)}{dz} = 1$. By Grönwall's inequality,

$$\left| \frac{d\hat{\psi}_{(u,1),t}(z)}{dz} \right| \leq \exp((1-u)L_1).$$

Combine the above inequalities with the previous Alekseev–Gröbner formula,

$$\begin{aligned} & \mathbb{E}_{X_i} \int_0^1 \delta_t^2(X_i(t)) dt \\ & \lesssim \mathbb{E}_{X_i} \int_0^1 \int_0^1 \left(\hat{V}(1-u, t, \psi_{u,t}(X_i(t))) - V(1-u, t, \psi_{u,t}(X_i(t))) \right)^2 du dt \\ & = \mathbb{E}_{X_i} \int_0^1 \int_0^1 \left(\hat{V}(u, t, \psi_{1-u,t}(X_i(t))) - V(u, t, \psi_{1-u,t}(X_i(t))) \right)^2 du dt \end{aligned}$$

It is worth noting that $\psi_{1-u,t}(X_i(t))$ follows the same density as $Z_u(t)$, by Theorem 3. Therefore,

$$\begin{aligned} \mathbb{E}_{X_i} \int_0^1 \delta_t^2(X_i(t)) dt & \lesssim \int_0^1 \mathbb{E}_{T, Z_u} \left\{ \hat{V}(u, T, Z_u(T)) - V(u, T, Z_u(T)) \right\}^2 du \\ & = o_p(1), \end{aligned}$$

according to (34).

– Notice that

$$|\psi_{1,t}(z)| = \left| z - \int_0^1 V(1-u, t, \psi_{u,t}(z)) du \right| \leq |z| + C,$$

where C is a constant due to the uniform boundedness of the vector field V .

Then, $\int_0^1 \mathbb{E}_{X_i} \psi_{1,t}^2(X_i(t)) dt \lesssim \mathbb{E} \|X_i\|^2 + C$, which is bounded.

With the above proof,

$$\|A\| = o_p(1)$$

due to (39). We similarly prove that $\|B\| = o_p(1)$ and $\|C\| = o_p(1)$. Thus:

$$\|\tilde{\rho} - \rho\| = o_p(1),$$

by (38).

- Given $L_\rho \rightarrow \infty$, $L_\rho = o(n^{1/2})$, and $\max\{\lambda_1, \lambda_2\} = o(1)$, we can show that

$$\|\hat{\rho} - \tilde{\rho}\|^2 = o_p(1).$$

The proof can be established using standard M-estimation theory ([Van der Vaart, 2000](#)), similar to the proof for the vector field V . We omit it here.

Consistency of functional data generation. Recall:

- $X(t) = \phi_{1,t}(Z(t))$, where $Z(t)$ is a mean-zero Gaussian process on \mathcal{T} with covariance function $\rho(t, s)$.
- $\tilde{X}(t) = \hat{\phi}_{1,t}(\tilde{Z}(t))$, where $\tilde{Z}(t)$ is a mean-zero Gaussian process on \mathcal{T} with covariance function $\hat{\rho}(t, s)$.

To bound $W_2(X, \tilde{X})$, we introduce an intermediate process:

$$Y(t) = \phi_{1,t}(\tilde{Z}(t))$$

and apply the triangle inequality in the Wasserstein metric:

$$W_2(X, \tilde{X}) \leq W_2(X, Y) + W_2(Y, \tilde{X}).$$

In the following, we respectively prove that $W_2(X, Y)$ and $W_2(Y, \tilde{X})$ are $o_p(1)$, which completes our proof.

- Consider $X(t) = \phi_{1,t}(Z(t))$ and $Y(t) = \phi_{1,t}(\tilde{Z}(t))$. From the flow equation:

$$\frac{\partial \phi_{u,t}(x)}{\partial u} = V_{u,t}(\phi_{u,t}(x)), \quad \phi_{0,t}(x) = x,$$

where $V_{u,t}(x)$ is Lipschitz in x with constant L . By (28), we have that

$$|\phi_{1,t}(x) - \phi_{1,t}(y)| \leq e^L |x - y|.$$

We denote $\rho^{1/2}$ and $\hat{\rho}^{1/2}$ as the square roots of the positive-definite kernels ρ and $\hat{\rho}$, respectively. Given this, we utilize the coupling $(X, Y) = (\phi_{1,\cdot}(Z), \phi_{1,\cdot}(\tilde{Z}))$, where $Z(t) = \int_{\mathcal{T}} \rho^{1/2}(t, s) N(s) \, ds$ and $\tilde{Z}(t) = \int_{\mathcal{T}} \hat{\rho}^{1/2}(t, s) N(s) \, ds$, with N being a mean-zero Gaussian process with covariance $\mathbb{I}(t = s)$. Accordingly,

$$\begin{aligned} W_2^2(X, Y) &\leq \mathbb{E} \|X - Y\|^2 \\ &\leq e^{2L} \cdot \mathbb{E} \|Z - \tilde{Z}\|^2 \\ &= e^{2L} \cdot \mathbb{E} \left\| \int_{\mathcal{T}} (\rho^{1/2}(t, s) - \hat{\rho}^{1/2}(t, s)) N(s) \, ds \right\|^2 \\ &\leq e^{2L} \cdot \iint_{\mathcal{T}} (\rho^{1/2}(t, s) - \hat{\rho}^{1/2}(t, s))^2 \, dt ds. \end{aligned}$$

For the kernels $\rho(t, s)$ and $\hat{\rho}(t, s)$, we define their integral operators \mathcal{K} and $\hat{\mathcal{K}}$ (defined by $(\mathcal{K}f)(t) = \int_{\mathcal{T}} \rho(t, s) f(s) \, ds$). Consequently,

$$\begin{aligned} &\iint_{\mathcal{T}} (\rho^{1/2}(t, s) - \hat{\rho}^{1/2}(t, s))^2 \, dt ds \\ &= \text{trace}(\mathcal{K}) + \text{trace}(\hat{\mathcal{K}}) - 2\text{trace}((\mathcal{K}^{1/2} \hat{\mathcal{K}} \mathcal{K}^{1/2})^{1/2}). \end{aligned}$$

where $\text{trace}(\cdot)$ is the trace of an operator. Define

$$f(\hat{\mathcal{K}}, \mathcal{K}) := \text{trace}(\mathcal{K}) + \text{trace}(\hat{\mathcal{K}}) - 2\text{trace}((\mathcal{K}^{1/2} \hat{\mathcal{K}} \mathcal{K}^{1/2})^{1/2}).$$

By Theorem 8 in [Mallasto and Feragen \(2017\)](#), $f(\hat{\mathcal{K}}, \mathcal{K}) = o_p(1)$ if $\|\mathcal{K} - \hat{\mathcal{K}}\|_{\text{op}} = o_p(1)$, where $\|\mathcal{K}\|_{\text{op}}$ is the operator norm of \mathcal{K} defined by $\sup_{\{f; \|f\| \leq 1\}} \|\mathcal{K}f\|$. Notice that

$$\|\mathcal{K} - \hat{\mathcal{K}}\|_{\text{op}}^2 \leq \sup_{\{f; \|f\| \leq 1\}} \left\| \int_{\mathcal{T}} (\rho(\cdot, s) - \hat{\rho}(\cdot, s)) f(s) \, ds \right\|^2 \leq \|\rho - \hat{\rho}\|^2 = o_p(1),$$

where the "—" is achieved by (37). We finally obtain

$$W_2(X, Y) = o_p(1),$$

by combining the above inequalities.

- Consider $\tilde{X}(t) = \hat{\phi}_{1,t}(\tilde{Z}(t))$ and $Y(t) = \phi_{1,t}(\tilde{Z}(t))$, which share the same underlying process $\tilde{Z}(t)$. We use the coupling $(\tilde{X}, Y) = (\phi_{1,\cdot}(\tilde{Z}), \hat{\phi}_{1,\cdot}(\tilde{Z}))$, then the squared Wasserstein distance satisfies:

$$W_2^2(\tilde{X}, Y) \leq \mathbb{E}_{\tilde{Z}} [\|X - Y\|^2] = \mathbb{E}_{\tilde{Z}} \left[\int_{\mathcal{T}} |\phi_{1,t}(\tilde{Z}(t)) - \hat{\phi}_{1,t}(\tilde{Z}(t))|^2 dt \right].$$

Similar to (40), we apply the Alekseev–Gröbner formula and obtain

$$\begin{aligned} & \int_{\mathcal{T}} |\phi_{1,t}(\tilde{Z}(t)) - \hat{\phi}_{1,t}(\tilde{Z}(t))|^2 dt \\ & \leq \int_0^1 \int_0^1 \left(\frac{d\hat{\phi}_{(u,1),t}(x)}{dx} \Big|_{x=\phi_{u,t}(\tilde{Z}_i(t))} \right)^2 \\ & \quad \cdot \left(\hat{V}(u, t, \phi_{u,t}(\tilde{Z}(t))) - V(u, t, \phi_{u,t}(\tilde{Z}(t))) \right)^2 du dt, \end{aligned}$$

where $\hat{\phi}_{(u,v),t}(x)$ denotes the solution of (25) starting at u and ending at v , with initial value x . Notice that $\hat{\phi}_{(u,w),t}(x) = x + \int_u^w \hat{V}(v, t, \hat{\phi}_{(u,v),t}(x)) dv$,

$$\frac{d\hat{\phi}_{(u,w),t}(x)}{dx} = 1 + \int_u^w \frac{d\hat{V}(v, t, x)}{dx} \Big|_{x=\phi_{(u,v),t}(x)} \cdot \frac{d\hat{\phi}_{(u,v),t}(x)}{dx} dv.$$

Therefore,

$$\frac{d}{dw} \left| \frac{d\hat{\phi}_{(u,w),t}(x)}{dx} \right| \leq L_1 \cdot \left| \frac{d\hat{\phi}_{(u,w),t}(x)}{dx} \right|,$$

due to the Lipschitz condition on \hat{V} . By Grönwall's inequality,

$$\left| \frac{d\hat{\phi}_{(u,w),t}(x)}{dx} \right| \leq \exp((w - u)L_1).$$

Combine the above inequalities with the previous Alekseev–Gröbner formula,

$$\begin{aligned}
W_2^2(\tilde{X}, Y) &\leq \mathbb{E}_{\tilde{z}} \int_{\mathcal{T}} |\phi_{1,t}(\tilde{Z}(t)) - \hat{\phi}_{1,t}(\tilde{Z}(t))|^2 dt \\
&\lesssim \mathbb{E}_{\tilde{z}} \int_{\mathcal{T}} \int_0^1 \left(\hat{V}(u, t, \phi_{u,t}(\tilde{Z}(t))) - V(u, t, \phi_{u,t}(\tilde{Z}(t))) \right)^2 du dt \\
&= \int_0^1 \mathbb{E}_{T, Z_u} \left\{ \hat{V}(u, T, Z_u(T)) - V(u, T, Z_u(T)) \right\}^2 du \\
&= o_p(1),
\end{aligned}$$

where the final ”=” is obtained from (34).

□

A.7 Additional Lemmas

Lemma S1. Let X be a random variable with a continuous and strictly increasing distribution function on an interval $\text{supp}(X) \subseteq \mathbb{R}$, with $\mathbb{P}(X \in \text{supp}(X)) = 1$. Suppose T and S are two continuous and strictly increasing functions on $\text{supp}(X)$. If the distributions of $T(X)$ and $S(X)$ are the same, then

$$T(X) = S(X)$$

almost surely.

Proof. Let F_X denote the CDF of X , which is continuous and strictly increasing on $\text{supp}(X)$. Define the intervals $I_T = \{T(x) \mid x \in \text{supp}(X)\}$ and $I_S = \{S(x) \mid x \in \text{supp}(X)\}$. Since T and S are continuous and strictly increasing, and $\text{supp}(X)$ is an interval, I_T and I_S are intervals. Given $\mathbb{P}(X \in \text{supp}(X)) = 1$, it follows that $\mathbb{P}(T(X) \in I_T) = \mathbb{P}(S(X) \in I_S) = 1$.

For $y \in I_T$, since T is strictly increasing, its inverse T^{-1} exists, and the event $\{T(X) \leq$

$y\}$ is equivalent to $\{X \leq T^{-1}(y)\}$. Thus,

$$\mathbb{P}(T(X) \leq y) = \mathbb{P}(X \leq T^{-1}(y)) = F_X(T^{-1}(y)).$$

Similarly, for $y \in I_S$,

$$\mathbb{P}(S(X) \leq y) = \mathbb{P}(X \leq S^{-1}(y)) = F_X(S^{-1}(y)).$$

Since $T(X)$ and $S(X)$ have the same distribution, their CDFs are equal for all y in their common domain. Moreover, because the distributions are identical, their supports must coincide; that is, $I_T = I_S$ (if $I_T \neq I_S$, there would exist y where $\mathbb{P}(T(X) \leq y) \neq \mathbb{P}(S(X) \leq y)$, contradicting the assumption). Let $I = I_T = I_S$. Thus,

$$F_X(T^{-1}(y)) = F_X(S^{-1}(y)) \quad \text{for all } y \in I.$$

Since F_X is strictly increasing, it is injective. Hence, $F_X(T^{-1}(y)) = F_X(S^{-1}(y))$ implies

$$T^{-1}(y) = S^{-1}(y) \quad \text{for all } y \in I.$$

Let $\Omega_0 = \{\omega \in \Omega \mid X(\omega) \in \text{supp}(X)\}$, with $\mathbb{P}(\Omega_0) = 1$. For each $\omega \in \Omega_0$, set $x = X(\omega) \in \text{supp}(X)$. Then, $T(x) \in I$, and we have

$$S^{-1}(T(x)) = T^{-1}(T(x)) = x.$$

Applying S to both sides, so $T(x) = S(x)$. Thus, $T(X(\omega)) = S(X(\omega))$ for all $\omega \in \Omega_0$.

Notice that $\mathbb{P}(\Omega_0) = 1$,

$$T(X) = S(X) \quad \text{almost surely.}$$

The proof is complete. \square

Lemma S2 (Picard–Lindelöf Theorem in a Banach space). Let $(E, \|\cdot\|_E)$ be a Banach space, $t_0 \in \mathbb{R}$, $x_0 \in E$, and let $f : E \times \mathbb{R} \rightarrow E$ satisfy:

- For each $x \in E$, the function $t \mapsto f(x, t)$ is continuous.
- For each compact set $K \subset E$ and each compact interval $I \subset \mathbb{R}$, there exists $L \geq 0$ such that for all $x, y \in K$ and $t \in I$,

$$\|f(x, t) - f(y, t)\|_E \leq L\|x - y\|_E.$$

Then, there exists $\delta > 0$ such that the initial value problem

$$\frac{dx}{dt} = f(x, t), \quad x(t_0) = x_0$$

has a unique solution $x : [t_0 - \delta, t_0 + \delta] \rightarrow E$.

See Theorem 3.A in [Zeidler \(1985\)](#) for the detailed proof.

Lemma S3. Let X be a random variable with distribution μ , where μ is absolutely continuous with respect to the Lebesgue measure λ (i.e., $\mu \ll \lambda$), and μ has a density $f > 0$ on the support of X . If $T(X) = S(X)$ almost surely, then $T = S$ almost everywhere in $\text{supp}(X)$ with respect to the Lebesgue measure.

Proof. Suppose $T(X) = S(X)$ almost surely, meaning:

$$\mu(\{x : T(x) \neq S(x)\}) = 0$$

Define $A = \{x \in \text{supp}(X) : T(x) \neq S(x)\}$. Since $A \subset \{x : T(x) \neq S(x)\}$ and $\mu(\{x : T(x) \neq S(x)\}) = 0$, it follows that:

$$\mu(A) = 0.$$

Given $\mu \ll \lambda$, we have $\mu(A) = \int_A f(x) d\lambda(x)$. Notice that $A \subset \text{supp}(X)$ and $f > 0$ on $\text{supp}(X)$. If $\lambda(A) > 0$, then:

$$\mu(A) = \int_A f(x) d\lambda(x) > 0.$$

This contradicts $\mu(A) = 0$. Hence, $\lambda(A) = 0$, proving that:

$$\lambda(\{x \in \text{supp}(X) : T(x) \neq S(x)\}) = 0$$

Thus, $T = S$ almost everywhere on $\text{supp}(X)$ with respect to the Lebesgue measure. \square

B Additional Technical Details

B.1 Smooth Flow Matching for Student- t Copula Processes

We extend SFM to general bases, enabling the model to capture more complex dependencies, such as tail dependence, the tendency for extreme values to occur simultaneously within a process (Staicu et al., 2012). In particular, we go beyond Gaussian bases by adopting the Student- t copula framework described in the following example. Additional extensions of SFM to broader copula structures are discussed in Part B.2.

A t -copula process is characterized by its degrees of freedom ν and a latent correlation function ρ . See the following example.

Example 3 (Student- t Copula Process). *Denote T_ν as the Student- t distribution with degrees of freedom $\nu > 0$. Let $\mathbf{T}_{\nu,\rho}(\cdot; t_1, \dots, t_m)$ be the joint distribution function of a mean-zero multivariate Student- t process with degrees of freedom $\nu > 0$ and correlation function ρ , evaluated at t_1, \dots, t_m . Set $F_{t,\text{base}} = T_\nu$, $t \in \mathcal{T}$, and $H_{\text{base}}(\cdot; t_1, \dots, t_m) = \mathbf{T}_{\nu,\rho}(\cdot; t_1, \dots, t_m)$, $t_1, \dots, t_m \in \mathcal{T}$. A stochastic process $X(\cdot)$ constructed with this base is called a Student- t copula process. By the property of the multivariate t -distribution, we have*

$$\rho(t, s) = \frac{\nu - 2}{\nu} \cdot \mathbb{E}\{T_\nu^{-1} \circ F_t(X(t)) \cdot T_\nu^{-1} \circ F_t(X(s))\}, \quad t, s \in \mathcal{T}, \nu > 2, \quad (41)$$

When $\nu \rightarrow \infty$, the t -copula process converges to the Gaussian copula process.

We provide the full procedure for smooth flow matching of Student- t copula processes in Algorithm S1 of the Supplementary Materials. The key modifications include:

- For any pair of observation times (T_{ij_1}, T_{ij_2}) we empirically estimate

$$\begin{aligned} & G_i^{(t\text{-copula})}(T_{ij_1}, T_{ij_2}) \\ &= \frac{\nu - 2}{\nu} \left\{ T_\nu^{-1} \circ \Phi \circ \hat{\psi}_{1, T_{ij_1}}(X_i(T_{ij_1})) \right\} \left\{ T_\nu^{-1} \circ \Phi \circ \hat{\psi}_{1, T_{ij_2}}(X_i(T_{ij_2})) \right\} \end{aligned} \quad (42)$$

based on (41). Surface-smoothing the collection $\{G_i^{(t\text{-copula})}(T_{ij_1}, T_{ij_2})\}_{i,j_1,j_2}$ yields a smooth estimator $\hat{\rho}(t, s)$ analogous to (24).

- Let $\tilde{V}_0^{(l)} \sim \mathbf{T}_{\nu, \hat{\rho}}$ be a mean-zero t -process with correlation $\hat{\rho}$. It can be simulated via

$$\tilde{V}_0^{(l)}(t) = \frac{W^{(l)}(t)}{\sqrt{u^{(l)}/\nu}}, \quad t \in \mathcal{T},$$

where $W^{(l)}$ is a zero-mean Gaussian process with covariance $\hat{\rho}$, $u^{(l)} \sim \chi_\nu^2$, and $W^{(l)}$ is independent of $u^{(l)}$.

- Set $\tilde{Z}_0^{(l)}(t) = \Phi^{-1} \circ T_\nu(\tilde{V}_0^{(l)}(t))$, where $\tilde{Z}_0^{(l)} \in W_2^2(\mathcal{T})$ since $\hat{\rho}$ satisfies the conditions of Example 2.

When $\nu \rightarrow \infty$, Algorithm S1 to the Gaussian-base in Algorithm 1. Practical estimation of ν from data is discussed in Part B.3.

B.2 Extensions of Smooth Flow Matching to General Copula

We next show how SFM can accommodate a general class of copula processes. By Sklar's theorem (Jaworski et al., 2010, see Supplementary Section B.4), the joint density of the irregular observations $\{X_i(T_{i1}), \dots, X_i(T_{iJ_i})\}$ satisfies

$$p_{X_i(T_{i1}), \dots, X_i(T_{iJ_i})}(x_1, \dots, x_{J_i}) = c_{T_{i1}, \dots, T_{iJ_i}}^d(F_{T_{i1}}(x_1), \dots, F_{T_{iJ_i}}(x_{J_i})) \prod_{j=1}^{J_i} p_{T_{ij}}(x_j), \quad (43)$$

Algorithm S1 Smooth Flow Matching for Student- t Copula Processes

1: **Input:** Observed data $\{(X_i(T_{ij}), T_{ij}); i = 1, \dots, n, j = 1, \dots, J_i\}$, number of samples H for estimation, number of samples M for generation, and the degree of freedom $\nu > 2$. A regularly spaced time grid \mathcal{T}_r such that $\cup_{i=1}^n \{T_{ij}; j \in [J_i]\} \subset \mathcal{T}_r$.

2: Generate H independent and identical mean-zero Gaussian processes, $Z_0^{(h)}$, $h = 1, \dots, H$, sampled at the time grid \mathcal{T}_r , with the covariance function being $\mathbb{I}(t = s)$.

3: Obtain the vector field \hat{V} from given the generated data $Z_0^{(h)}(t)$, $h = 1, \dots, H$, and $t \in \mathcal{T}_r$:

$$\hat{V} := \operatorname{argmin}_{U \in \mathbb{B}_{L,4}([0,1], \mathcal{T}, \mathcal{X})} \{\hat{\mathcal{L}}(U) + \mathcal{J}(U)\}.$$

4: Calculate $G_i^{(t\text{-copula})}(T_{ij_1}, T_{ij_2})$

$$G_i^{(t\text{-copula})}(T_{ij_1}, T_{ij_2}) = \frac{\nu - 2}{\nu} \cdot \mathbf{T}_\nu^{-1} \circ \Phi \circ \hat{\psi}_{1,T_{ij_1}}(X_i(T_{ij_1})) \cdot \mathbf{T}_\nu^{-1} \circ \Phi \circ \hat{\psi}_{1,T_{ij_2}}(X_i(T_{ij_2})),$$

where $\hat{\psi}_{1,t}(z)$ is the solution of $\frac{\partial \hat{\psi}_{u,t}(z)}{\partial u} = -\hat{V}(1 - u, t, \hat{\psi}_{u,t}(z))$, subject to $\hat{\psi}_{0,t}(z) = z$.

5: Apply surface smoothing on $\{G_i^{(t\text{-copula})}(T_{ij_1}, T_{ij_2}); i = 1, \dots, n, j_1, j_2 = 1, \dots, J_i\}$ to obtain $\hat{\rho}(t, s)$.

6: Regenerate M independent and identical mean-zero Gaussian processes, $\tilde{W}_0^{(l)}$, $l = 1, \dots, L$, sampled at the time grid \mathcal{T}_r , with the covariance function being $\hat{\rho}(t, s)$, and $u^{(l)} \sim \chi_\nu^2$, $l = 1, \dots, L$.

7: For $l = 1, \dots, L$ and $t \in \mathcal{T}_r$, solve the equation

$$\frac{\partial \tilde{Z}_u^{(l)}(t)}{\partial u} = \hat{V}(u, t, \tilde{Z}_u^{(l)}(t))$$

given the initial value $\tilde{Z}_0^{(l)}(t) = \Phi^{-1} \circ \mathbf{T}_\nu \left(\frac{W^{(l)}(t)}{\sqrt{u^{(l)}/\nu}} \right)$, obtaining $\tilde{Z}_1^{(l)}(t)$ for each $t \in \mathcal{T}$.

8: **Output:** $\tilde{Z}_1^{(l)}(t)$, $t \in \mathcal{T}_r$ and $l = 1, \dots, L$.

where $F_{T_{ij}}$ and $p_{T_{ij}}$ are the marginal CDF and density, while $c_{T_{i1}, \dots, T_{iJ_i}}^d$ is the copula density $\partial^{J_i} c_{T_{i1}, \dots, T_{iJ_i}} / \partial u_1 \cdots \partial u_{J_i}$. For any m -tuple $(t_1, \dots, t_m) \subset \mathcal{T}$, we express the copula c_{t_1, \dots, t_m}

via a base joint distribution H_{base} based on Definition 1:

$$c_{t_1, \dots, t_m}(u_1, \dots, u_m) = H_{\text{base}}(F_{t_1, \text{base}}^{-1}(u_1), \dots, F_{t_m, \text{base}}^{-1}(u_m); t_1, \dots, t_m),$$

where $F_{t, \text{base}}$ denotes the marginal base cumulative distribution function.

Let $H_{\text{base}, \theta}$ be a parametric family indexed by $\theta \in \Theta$. Combining (43) with the above representation yields the log-likelihood of θ :

$$\begin{aligned} & \ell\left(\{X_i(T_{ij})\}; \theta\right) \\ &= \sum_{i=1}^n \log \left[\frac{\partial^{J_i} H_{\text{base}, \theta}(F_{T_{i1}, \text{base}}^{-1}(u_1), \dots, F_{T_{iJ_i}, \text{base}}^{-1}(u_{J_i}); T_{i1}, \dots, T_{iJ_i})}{\partial u_1 \cdots \partial u_{J_i}} \right]_{u_j=F_{T_{ij}}(X_i(T_{ij}))} \\ &= \sum_{i=1}^n \log \left[\frac{\partial^{J_i} H_{\text{base}, \theta}(z_1, \dots, z_{J_i}; T_{i1}, \dots, T_{iJ_i})}{\partial z_1 \cdots \partial z_{J_i}} \right]_{z_j=F_{T_{i1}, \text{base}}^{-1} \circ F_{T_{ij}}(X_i(T_{ij}))} + C, \end{aligned} \quad (44)$$

where C contains the terms independent of θ . Hence ℓ depends on θ and the unknown transformations $F_{t, \text{base}}^{-1} \circ F_t$, $t \in \mathcal{T}$. Estimating θ while treating the latter nonparametrically constitutes a semiparametric copula problem (Jaworski et al., 2010).

Therefore, we introduce the following practical estimation steps.

1. Specify marginals: Fix base process $F_{t, \text{base}}$ (e.g., Gaussian) for every $t \in [0, 1]$.
2. Estimate transformations: Using the smooth vector field from (20), solve the backward ordinary differential equation in (22) with initial value $X_i(T_{ij})$ to obtain $F_{T_{ij}, \text{base}}^{-1} \circ F_{T_{ij}}(X_i(T_{ij}))$.
3. Estimate copula parameter: Substitute these quantities into (44) and maximize over θ to obtain $\hat{\theta}$.
4. Generate new samples: Draw $\tilde{Z}_0 \sim H_{\text{base}, \hat{\theta}}$, and solve the forward ordinary differential equation (25) to simulate new functional data.

We summarize the entire workflow in Algorithm S2.

Algorithm S2 Smooth Flow Matching for General Copula Processes

- 1: **Input:** Observed data $\{(X_i(T_{ij}), T_{ij}); i = 1, \dots, n, j = 1, \dots, J_i\}$, number of samples H for estimation, number of samples M for generation, and base distributions $F_{t, \text{base}}$, $t \in \mathcal{T}$.
- 2: **Input:** A regularly spaced time grid \mathcal{T}_r such that $\cup_{i=1}^n \{T_{ij}; j \in [J_i]\} \subset \mathcal{T}_r$.
- 3: Generate H independent and identically distributed base processes: $Z_0^{(h)}(t) \sim F_{t, \text{base}}$, for $h = 1, \dots, H$, and $t \in \mathcal{T}_r$
- 4: Obtain the vector field \hat{V} from given the generated data $Z_0^{(h)}(t)$, $h = 1, \dots, H$, and $t \in \mathcal{T}_r$:

$$\hat{V} := \operatorname{argmin}_{U \in \mathbb{B}_{L,4}([0,1], \mathcal{T}, \mathcal{X})} \{\hat{\mathcal{L}}(U) + \mathcal{J}(U)\}.$$

- 5: Calculate $\hat{\theta}$ by

$$\arg \max_{\theta} \sum_{i=1}^n \log \left[\frac{\partial^{J_i} H_{\text{base}, \theta}(z_1, \dots, z_{J_i}; T_{i1}, \dots, T_{iJ_i})}{\partial z_1 \cdots \partial z_{J_i}} \right]_{z_j=\hat{\psi}_{1, T_{ij}}(X_i(T_{ij}))},$$

where $\hat{\psi}_{1,t}(z)$ is the solution of $\frac{\partial \hat{\psi}_{u,t}(z)}{\partial u} = -\hat{V}(1-u, t, \hat{\psi}_{u,t}(z))$, subject to $\hat{\psi}_{0,t}(z) = z$.

- 6: Regenerate L independent and identical processes, $\tilde{Z}_0^{(l)}$, $l = 1, \dots, L$, sampled at the time grid \mathcal{T}_r , according to the joint distribution $H_{\text{base}, \hat{\theta}}$.
- 7: For $l = 1, \dots, L$ and $t \in \mathcal{T}_r$, solve the equation

$$\frac{\partial \tilde{Z}_u^{(l)}(t)}{\partial u} = \hat{V}(u, t, \tilde{Z}_u^{(l)}(t))$$

given the initial value $\tilde{Z}_0^{(l)}(t)$, obtaining $\tilde{Z}_1^{(l)}(t)$ for each $t \in \mathcal{T}$.

- 8: **Output:** $\tilde{Z}_1^{(l)}(t)$, $t \in \mathcal{T}_r$ and $l = 1, \dots, L$.

B.3 Degrees of Freedom in Student t -Copula Processes

In this section, we focus on estimating the degrees of freedom ν for a t -copula process, based on the observed data $\{(X_i(T_{ij}), T_{ij}) : i = 1, \dots, n, j = 1, \dots, J_i\}$. Since the observed time points T_{ij} vary across subjects, we first transform the time points by rounding them to an equally spaced dense grid over the interval $[0, 1]$ that includes all observed time points $\{T_{ij} : i = 1, \dots, n; j = 1, \dots, J_i\}$. For each subject i and each time point t on this grid,

we preprocess the observed data by: (1) assigning the value $X_i(T_{ij})$ if $T_{ij} = t$; or, if no such value exists, (2) marking the data as missing. This results in n random vectors with missing entries, which are then used to estimate ν based on the partially observed data.

In the following, we estimate the degrees of freedom ν from multivariate t -copula data, following the method in [Demarta and McNeil \(2005\)](#). Let $\{\mathbf{x}_i\}_{i=1}^n$ denote n independent observations of a d -dimensional random vector, where each $\mathbf{x}_i = (x_i^{(1)}, \dots, x_i^{(d)}) \in \mathbb{R}^d$ may contain missing entries. We assume that \mathbf{x}_i follows a multivariate t -copula with base distribution $\mathbf{T}_{\nu, \Sigma}$, where ν is the degrees of freedom and $\Sigma = (\rho_{jk})_{j,k=1}^d$ is the correlation matrix. To handle the presence of missing data, we construct a composite pairwise likelihood to estimate the degrees of freedom ν .

For each pair of variables (j, k) with $1 \leq j < k \leq d$, define the index set

$$\mathcal{I}_{jk} = \left\{ i \in \{1, \dots, n\} : x_i^{(j)} \text{ and } x_i^{(k)} \text{ are both observed} \right\}.$$

To construct the pairwise composite likelihood, we first transform the data to the copula scale. For each variable j , we use the empirical cumulative distribution function:

$$\hat{F}_j(x) = \frac{1}{n_j} \sum_{i=1}^{n_j} \mathbb{I}\{x_i^{(j)} \leq x, x_i^{(j)} \text{ observed}\}, \quad n_j = \left| \{i : x_i^{(j)} \text{ observed}\} \right|.$$

Then, for each observation $i \in \mathcal{I}_{jk}$, we define the pseudo-observations:

$$u_i^{(j)} = \hat{F}_j(x_i^{(j)}), \quad u_i^{(k)} = \hat{F}_k(x_i^{(k)}).$$

The pairwise composite log-likelihood is then constructed by:

$$\ell_{\text{PCL}}(\nu, (\rho_{jk})_{j,k=1}^d) = \sum_{1 \leq j < k \leq d} \sum_{i \in \mathcal{I}_{jk}} \log c_{\nu} \left(u_i^{(j)}, u_i^{(k)}; \rho_{jk}, \nu \right),$$

where $c_{\nu}(u, v; \rho, \nu)$ is the density of the bivariate t -copula with correlation ρ and degrees of freedom ν . This density is given by:

$$c_{\nu}(u, v; \rho, \nu) = \frac{\mathbf{t}_{\nu, \rho}(\mathbf{T}_{\nu}^{-1}(u), \mathbf{T}_{\nu}^{-1}(v))}{\mathbf{t}_{\nu}(\mathbf{T}_{\nu}^{-1}(u)) \cdot \mathbf{t}_{\nu}(\mathbf{T}_{\nu}^{-1}(v))},$$

where $t_\nu(\cdot)$ is the density of the univariate t -distribution with ν degrees of freedom; $\mathbf{t}_{\nu,\rho}(\cdot, \cdot)$ is the bivariate t -density with degrees of freedom ν and correlation ρ . See Equation (6) in [Demarta and McNeil \(2005\)](#) for details.

To alleviate computation, we follow [Demarta and McNeil \(2005\)](#) and estimate ρ_{jk} using Kendall's tau correlation. Define the Kendall's tau $\hat{\tau}_{jk}$ between variables j and k as:

$$\hat{\tau}_{jk} = \frac{2}{|\mathcal{I}_{jk}|(|\mathcal{I}_{jk}|-1)} \sum_{1 \leq r < s \leq |\mathcal{I}_{jk}|} \text{sign}((x_r^{(j)} - x_s^{(j)})(x_r^{(k)} - x_s^{(k)})),$$

where the sum is taken over all distinct pairs of observations in \mathcal{I}_{jk} , the index set of complete cases for the pair (j, k) , and $\text{sign}(\cdot)$ denotes the sign function. According to Equation (9) in [Demarta and McNeil \(2005\)](#), the correlation ρ_{jk} is related to Kendall's tau by:

$$\rho_{jk} = \sin\left(\frac{\pi}{2} \mathbb{E}[\hat{\tau}_{jk}]\right).$$

Thus, an estimate of ρ_{jk} can be obtained as:

$$\hat{\rho}_{jk} = \sin\left(\frac{\pi}{2} \hat{\tau}_{jk}\right).$$

By plugging in these estimates, the degrees of freedom ν is obtained by maximizing the composite log-likelihood:

$$\hat{\nu} = \arg \max_{\nu > 2} \ell_{\text{PCL}}(\nu, (\hat{\rho}_{jk})_{j,k=1}^d).$$

B.4 Sklar's Theorem

Sklar's Theorem is a fundamental result in the theory of copulas, providing a crucial link between multivariate distribution functions and their univariate margins.

Theorem 5 (Sklar's Theorem). Let H be an n -dimensional joint cumulative distribution function (CDF) with marginals F_1, F_2, \dots, F_n . Then there exists a copula $C : [0, 1]^n \rightarrow [0, 1]$

such that for all $x_1, x_2, \dots, x_n \in \mathbb{R}$,

$$H(x_1, x_2, \dots, x_n) = C(F_1(x_1), F_2(x_2), \dots, F_n(x_n)).$$

If each F_i is continuous, then the copula C is unique. Conversely, if C is a copula and F_1, \dots, F_n are univariate CDFs, then the function H defined by the above equation is a joint CDF with marginals F_1, \dots, F_n .

Assume that H is absolutely continuous with joint probability density function h , and that each marginal F_i is absolutely continuous with density f_i . Then, under regularity conditions, the copula C is also differentiable, and Sklar's Theorem can be expressed in terms of densities as follows:

$$h(x_1, x_2, \dots, x_n) = c(F_1(x_1), F_2(x_2), \dots, F_n(x_n)) \cdot f_1(x_1) \cdot f_2(x_2) \cdots f_n(x_n),$$

where $c(u_1, u_2, \dots, u_n)$ is the density of the copula C , defined by

$$c(u_1, u_2, \dots, u_n) = \frac{\partial^n}{\partial u_1 \partial u_2 \cdots \partial u_n} C(u_1, u_2, \dots, u_n).$$

B.5 Restricted Maximum Likelihood

Recall that the loss function in (20) is defined as

$$\begin{aligned} & \frac{1}{nHF} \sum_{i=1}^n \frac{1}{J_i} \sum_{j=1}^{J_i} \sum_{h=1}^H \sum_{f=1}^F \left[X_i(T_{ij}) - Z_0^{(h)}(T_{ij}) - U(u_f, T_{ij}, Z_{u_f, i}^{(h)}(T_{ij})) \right]^2 \\ & + \int_{\mathcal{X}} \int_{\mathcal{T}} \int_0^1 \lambda_u \left(\frac{\partial^2 U}{\partial u^2} \right)^2 + \lambda_t \left(\frac{\partial^2 U}{\partial t^2} \right)^2 + \lambda_x \left(\frac{\partial^2 U}{\partial x^2} \right)^2 \, du dt dx \end{aligned} \quad (45)$$

Denote the tensor-product basis for U as $\{\psi_k(u, t, x)\}_{k=1}^K$, and write

$$U(u, t, x) = \sum_{k=1}^K \beta_k \psi_k(u, t, x), \quad \boldsymbol{\beta} = (\beta_1, \dots, \beta_K)^\top.$$

Stack every residual $y_{ijhf} = X_i(T_{ij}) - Z_0^{(h)}(T_{ij})$ into $\mathbf{y} \in \mathbb{R}^m$, with $m = \sum_{i=1}^n J_i HF$. Define the design matrix

$$\mathbf{W}_{(ijhf),k} = \psi_k(u_f, T_{ij}, Z_{u_f, i}^{(h)}(T_{ij})),$$

and introduce the diagonal weight matrix

$$\mathbf{D} = \text{diag}(d_{ijhf}), \quad d_{ijhf} = 1/(nHFJ_i).$$

Utilizing the above notation, we formulate (45) as

$$\left\| \mathbf{D}^{1/2}(\mathbf{y} - \mathbf{W}\boldsymbol{\beta}) \right\|^2 + \boldsymbol{\beta}^\top (\lambda_u R_u + \lambda_t R_t + \lambda_x R_x) \boldsymbol{\beta}, \quad (46)$$

where the penalty matrices R_u, R_t, R_x are as given as

$$\begin{aligned} (R_u)_{kl} &= \int_{\mathcal{X}} \int_{\mathcal{T}} \int_0^1 \frac{\partial^2 \psi_k}{\partial u^2}(u, t, x) \frac{\partial^2 \psi_l}{\partial u^2}(u, t, x) du dt dx, \\ (R_t)_{kl} &= \int_{\mathcal{X}} \int_{\mathcal{T}} \int_0^1 \frac{\partial^2 \psi_k}{\partial t^2}(u, t, x) \frac{\partial^2 \psi_l}{\partial t^2}(u, t, x) du dt dx, \\ (R_x)_{kl} &= \int_{\mathcal{X}} \int_{\mathcal{T}} \int_0^1 \frac{\partial^2 \psi_k}{\partial x^2}(u, t, x) \frac{\partial^2 \psi_l}{\partial x^2}(u, t, x) du dt dx. \end{aligned}$$

Consider the model

$$\mathbf{y} \mid \boldsymbol{\beta}, \sigma^2 \sim N(\mathbf{W}\boldsymbol{\beta}, \sigma^2 \mathbf{D}^{-1})$$

with the prior

$$\boldsymbol{\beta} \mid \sigma^2, \lambda_u, \lambda_t, \lambda_x \sim \text{Gau}\left(\mathbf{0}, \sigma^2 [\lambda_u R_u + \lambda_t R_t + \lambda_x R_x]^{-1}\right).$$

The negative log-posterior of $\boldsymbol{\beta}$, up to an additive constant, is the same as (46); hence, the original minimizer coincides with the Maximum A Posteriori (MAP) estimator in the Bayesian model.

To obtain the tuning parameters $\lambda := \{\lambda_u, \lambda_t, \lambda_x\}$, we integrate out $\boldsymbol{\beta}$ and obtain:

$$\mathbf{y} \mid \sigma^2, \lambda \sim \text{Gau}(\mathbf{0}, \sigma^2 \mathbf{V}(\lambda)),$$

where

$$\mathbf{V}(\lambda) = \mathbf{D}^{-1} + \mathbf{W} \mathbf{G}(\lambda) \mathbf{W}^\top, \quad \mathbf{G}(\lambda) = [\lambda_u R_u + \lambda_t R_t + \lambda_x R_x]^{-1}.$$

The likelihood for λ and σ is then established by

$$\ell_R(\lambda_u, \lambda_t, \lambda_x, \sigma^2) = -\frac{1}{2} \left[m \log \sigma^2 + \log |\mathbf{V}(\lambda)| + \frac{1}{\sigma^2} \mathbf{y}^\top \mathbf{V}^{-1}(\lambda) \mathbf{y} \right].$$

Profiling out σ^2 yields

$$\hat{\sigma}^2(\lambda) = \frac{\mathbf{y}^\top \mathbf{V}(\lambda)^{-1} \mathbf{y}}{m},$$

which leads to the likelihood of λ :

$$\tilde{\ell}_R(\lambda_u, \lambda_t, \lambda_x) = -\frac{1}{2} \left[m \log \{ \mathbf{y}^\top \mathbf{V}^{-1}(\lambda) \mathbf{y} \} + \log |\mathbf{V}(\lambda)| \right].$$

Maximising the above likelihood gives the REML estimates $\hat{\lambda}_u, \hat{\lambda}_t, \hat{\lambda}_x$.

B.6 Regression Procedure for Data Prediction

In real data analysis, we estimate f by minimizing the penalized squared error loss:

$$\hat{f} = \arg \min_{f \in \mathbb{B}_{L,4}(\text{supp}(X), \mathcal{T})} \sum_{i \in \mathcal{E}} \sum_{j=1}^{30} \{X_i(T_{j+1}) - f(X_i(T_j), T_j)\}^2 \cdot \mathcal{I}_{T_j, T_{j+1}}(X_i) + \mathcal{J}(f),$$

where \mathcal{E} indexes the training set, $\mathcal{I}_{T_j, T_{j+1}}(X_i) = 1$ if X_i is observed at both T_j and T_{j+1} , and 0 otherwise. We set $L = 5$ for the spline basis, and $\mathcal{J}(f)$ denotes a roughness penalty similar to (24). We estimate \hat{f} using the R package `mgcv` (Wood and Wood, 2015).

C Supporting Results

C.1 MSE for Mean, Eigen, and Median Function Estimation

We present the mean squared errors (MSE) between the true mean function (MF), eigenfunctions (EF), and median function (MDF) and their corresponding estimates obtained

from raw data and from generated data in the simulation study, as summarized in Table C.1. Note that the MDF values are not presented for the Gaussian process case (A), since for this case the mean and median coincide, implying that $MDF = MF$ in these scenarios. Meanwhile, the MDF values are not presented for the Oracle case, as the oracle method ([Hsing and Eubank, 2015](#)) is not designed for MDF estimation.

Table 4: Mean squared errors (MSE) between the true mean function (MF), eigenfunctions (EF), median function (MDF), and their estimates from raw/generated data. "Oracle" refers to MF/EF estimated directly from observed data using the smoothing method of [Hsing and Eubank \(2015\)](#).

MSE			{2, ..., 6}				{6, ..., 10}			
			MF	EF1	EF2	MDF	MF	EF1	EF2	MDF
(A)	$n = 100$	DSM	0.55	1.08	1.07		0.23	1.19	1.19	
		FM	0.99	1.02	1.01		0.46	1.20	0.98	
		GP	0.17	0.54	0.67		0.15	0.41	0.55	
		KL	0.17	0.56	0.71		0.15	0.47	0.64	
		SFM	0.18	0.46	0.58		0.16	0.42	0.59	
		Oracle	0.14	0.48	0.62		0.11	0.35	0.48	
	$n = 200$	DSM	0.63	1.16	1.15		0.25	1.26	1.23	
		FM	0.79	1.04	1.00		0.34	1.20	1.03	
		GP	0.15	0.47	0.55		0.14	0.42	0.55	
		KL	0.14	0.50	0.64		0.13	0.43	0.56	
		SFM	0.15	0.46	0.56		0.13	0.41	0.52	
		Oracle	0.10	0.38	0.49		0.08	0.28	0.37	
(B)	$n = 300$	DSM	0.59	1.18	1.14		0.25	1.28	1.21	
		FM	0.95	1.06	1.01		0.36	1.19	1.03	
		GP	0.13	0.42	0.53		0.12	0.41	0.51	
		KL	0.14	0.38	0.48		0.12	0.40	0.49	
		SFM	0.12	0.44	0.54		0.11	0.36	0.45	
		Oracle	0.09	0.30	0.38		0.07	0.23	0.30	
	$n = 100$	DSM	0.16	0.69	0.63	0.17	0.10	0.39	0.47	0.10
		FM	0.15	0.68	0.76	0.08	0.11	0.52	0.66	0.08
		GP	0.11	0.40	0.52	0.29	0.10	0.37	0.45	0.30
		KL	0.12	0.47	0.60	0.29	0.10	0.39	0.52	0.29
		SFM	0.12	0.44	0.54	0.14	0.10	0.37	0.47	0.12
		Oracle	0.09	0.46	0.58		0.07	0.38	0.49	
(B)	$n = 200$	DSM	0.13	0.69	0.59	0.14	0.10	0.33	0.38	0.12
		FM	0.14	0.71	0.73	0.07	0.10	0.34	0.48	0.07
		GP	0.09	0.32	0.43	0.29	0.09	0.28	0.38	0.28
		KL	0.09	0.38	0.50	0.28	0.08	0.33	0.43	0.28
		SFM	0.10	0.36	0.43	0.11	0.08	0.32	0.41	0.09
		Oracle	0.06	0.36	0.46		0.05	0.30	0.39	
	$n = 300$	DSM	0.16	0.68	0.56	0.16	0.11	0.35	0.44	0.12
		FM	0.13	0.58	0.61	0.09	0.10	0.32	0.44	0.08
		GP	0.08	0.30	0.38	0.29	0.08	0.26	0.33	0.29
		KL	0.08	0.35	0.46	0.28	0.07	0.30	0.40	0.29
		SFM	0.10	0.32	0.38	0.11	0.08	0.29	0.36	0.09
		Oracle	0.05	0.31	0.41		0.04	0.24	0.33	

C.2 Sensitivity Analysis of Noise

Following the Gamma process model in Section 5, we generate noisy observations as $Y_{ij} = X_i(T_{ij}) + \tau_{ij}$, for $i = 1, \dots, n$ and $j = 1, \dots, J_i$, where τ_{ij} , $j = 1, \dots, J_i$ are independent mean-zero Gaussian noises with variance set to $\frac{1}{J_i} \sum_{j=1}^{J_i} X_i^2(T_{ij}) \times \text{noise level}$, for each i . Based on the noisy and irregular observations, we apply SFM to learn the vector field for data generation. In addition, we also apply SFM to the denoised data of Y_{ij} , obtained from Remark 4. The denoised values are then used as input for SFM. In Figure 7, we show the Wasserstein distances between the true data and the generated data from SFM with noisy or denoised input. We observe that the performance of SFM slightly deteriorates as the noise level increases. In contrast, applying denoising to data prior to generation improves the performance of SFM, making it less sensitive to the added noise.

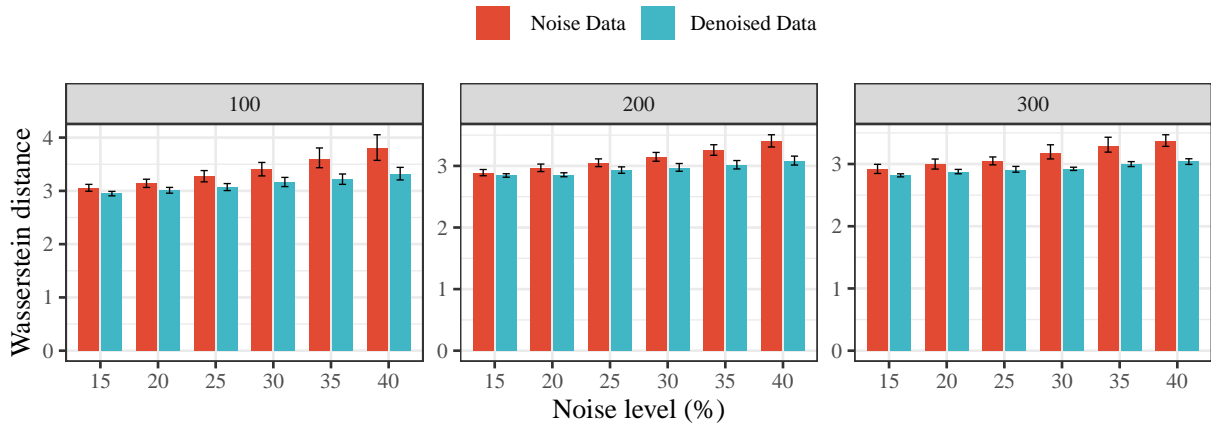


Figure 7: Wasserstein distances from 100 simulation replications under varying sample sizes n (indicated in titles) for $J_i \in \{6, \dots, 10\}$.